

MODIFYING THE STANDARD DISK MODEL FOR THE ULTRAVIOLET SPECTRAL ANALYSIS OF DISK-DOMINATED CATAclySMIC VARIABLES. I. THE NOVALIKES MV LYRAE, BZ CAMELOPARDALIS, AND V592 CASSIOPEIAE ¹

PATRICK GODON ², EDWARD M. SION

Astrophysics and Planetary Science, Villanova University, 800 Lancaster Ave., Villanova, PA 19085, USA

ŞÖLEN BALMAN

Department of Physics, Middle East Technical University, Ankara, Turkey

WILLIAM P. BLAIR

Henry A. Rowland Department of Physics & Astronomy, The Johns Hopkins University, Baltimore, MD 21218, USA

¹This e-print copy was not formatted nor edited for The Astrophysical Journal, the figures have been reduced to span only one column.

²Visiting in the Henry A. Rowland Department of Physics & Astronomy, The Johns Hopkins University, Baltimore, MD 21208

ABSTRACT

The standard disk is often inadequate to model disk-dominated cataclysmic variables (CVs) and generates a spectrum that is bluer than the observed UV spectra (Puebla et al. 2007). X-ray observations of these systems reveal an optically thin boundary layer (BL) expected to appear as an inner hole in the disk. Consequently, we truncate the inner disk. However, instead of removing the inner disk, we impose the no-shear boundary condition at the truncation radius, thereby lowering the disk temperature and generating a spectrum that better fits the UV data. With our modified disk, we analyze the archival UV spectra of three novalikes that cannot be fitted with standard disks. For the VY Scl systems MV Lyr and BZ Cam, we fit a hot inflated white dwarf WD with a cold modified disk ($\dot{M} \sim$ a few $10^{-9} M_{\odot}/\text{yr}$). For V592 Cas, the slightly modified disk ($\dot{M} \sim 6 \times 10^{-9} M_{\odot}/\text{yr}$) completely dominates the UV. These results are consistent with *Swift* X-ray observations of these systems (Balman et al. 2014), revealing BLs merged with ADAF-like flows and/or hot coronae, where the advection of energy is likely launching an outflow and heating the WD, thereby explaining the high WD temperature in VY Scl systems. This is further supported by the fact that the X-ray hardness ratio increases with the shallowness of the UV slope in a small CV sample we examine. Furthermore, for 105 disk-dominated systems, the *International Ultraviolet Explorer* (IUE) spectra UV slope decreases in the same order as the ratio of the X-ray flux to optical/UV flux: from SU UMa's, to U Gem's, Z Cam's, UX UMa's, and VY Scl's.

Keywords: accretion, accretion disks — novae, cataclysmic variables — white dwarfs

1. INTRODUCTION: ULTRAVIOLET DISK SPECTRA AND OPTICALLY THIN HARD X-RAY IN NOVALIKES

The properties of accretion disks in binary systems are best studied in the brightest types of non-magnetic cataclysmic variables (CVs): the novalikes (NLs) in high state and dwarf novae (DNe) in outburst. These systems are compact binaries with a white dwarf (WD) accreting matter and angular momentum via a disk from a

low-mass companion filling its Roche lobe. Dwarf nova systems are found mostly in a state of low mass accretion rate (quiescence) and have periods of high mass accretion rate (outburst) when the disk dominates the UV (Hack & la Dous 1993). NLs are found mostly in a state of high mass accretion in which the UV emission is predominantly originating from the disk (la Dous 1990, 1991). For that reason, the DNe in outburst and NLs in high state are of special interest because they are expected to have an accretion disk radial temperature profile given by the analytical expression $T_{\text{eff}}(R)$ of the standard disk model (Pringle 1981).

However, 30 years ago already, Wade (1984, 1988) showed, using *International Ultraviolet Explorer* (IUE) spectra, that some CV systems systematically disagree

patrick.godon@villanova.edu ; edward.sion@villanova.edu

solen@astroa.physics.metu.edu.tr

wpb@pha.jhu.edu

with the standard disk model when either black body or Kurucz stellar models were used to represent the accretion disk. A better model was developed by Hubeny (1990) explicitly including the calculation of synthetic spectra using the standard disk model (the code TLUSTY; Wade & Hubeny (1998)). This modeling was more successful and has been used since in standard procedures to assess the mass accretion rate of systems in a state of high mass accretion rate (e.g. Knigge & Long (2002); Hamilton et al. (2007)). With time, however, it appeared that a large fraction of disk systems could **not** be modeled using the standard disk temperature profile, and instead the temperature of the disk had to be modified, e.g. IX Vel, QU Car, RW Sex; Linnell et al. (2007, 2008, 2010). A statistical study (Puebla et al. 2007) of 33 disk systems indicated that a revision of the temperature profile, at least in the innermost part of the disk, is required: a large fraction of the theoretical spectra were too blue compared to the observed spectra. Some of the UV spectral modelings of disk-dominated systems that were in better agreement with the observations consisted of truncating the hot inner disk (Linnell et al. 2005). By truncating the hottest region in the disk, the slope of the UV continuum became shallower as the spectrum became redder. In her statistical analysis of *IUE* spectra of CVs, la Dous (1991) already pointed out that dwarf novae in outburst have a continuum flux level increasing toward the shorter wavelength (blue), while the continuum slope is shallower for non-magnetic NLs and it is almost flat for intermediate polars (IPs - systems in which the inner disk is expected to be truncated by the WD magnetic field). la Dous (1991) showed that *IUE* spectra of IPs were similar in slope/color to theoretical spectra of magnetically truncated disks with a truncation radius $\approx 5R_{\text{wd}}$, while in contrast, a large number of DNe in outburst have been successfully modeled with non-truncated standard disk spectra (Hamilton et al. 2007). This suggests that the disk spectra of non-magnetic NLs, showing a UV continuum slope intermediate between IPs and DNe in outburst, might have a truncated disk with a truncation radius smaller than in IPs.

In addition to the above problem in the UV spectroscopy of disk-dominated systems, X-ray data of CVs have also been in strong disagreement with the theoretical expectations for more than three decades (Ferland et al. 1982). The culprit has been the difficult to study boundary layer (BL) between the accretion disk and the WD. About half of the disk accretion energy (in the form of kinetic energy) is expected to be dissipated in the BL between the Keplerian disk and slowly rotating stellar surface (Pringle 1981). Because of its small size, the BL was predicted to emit in the X-ray band: at low accretion rates (when the WD is dominant in the UV), the BL was expected to be optically thin and emit hard X-rays (Pringle & Savonije 1979; Tytenda 1982; Narayan & Popham 1993); at large accretion rates, typical of NLs in a high state

and DNe in outburst, the BL was expected to be optically thick and emit soft X-rays (Pringle 1977; Narayan & Popham 1993; Popham & Narayan 1995). Systems in the low state indeed reveal optically thin hard X-ray emission (Szkody et al. 2002; Pandel et al. 2005; Mukai et al. 2009). However, systems in a state of high mass accretion often do not show an optically thick soft X-ray component; instead, many exhibit optically thin hard X-ray emission (Patterson & Raymond 1985a,b; Mauche et al. 1995; van Teeseling et al. 1996; Baskill et al. 2005; Balman et al. 2014), with an X-ray luminosity much smaller than expected, i.e. much smaller than the disk luminosity. While optically thin hard X-ray emission from high mass accretion rate systems was unexpected, it is, however, not especially inconsistent with the theoretical work: optically thin boundary layers can occur in high mass accretion rate systems, since the transition to optically thin depends not only on the mass accretion rate, but also on the WD mass, the WD rotation rate and the (unknown) alpha viscosity parameter (Popham & Narayan 1995). Simulations of optically thin BLs (Narayan & Popham 1993; Popham 1999) show that the inner edge of the Keplerian (and optically thick) disk starts at an actual radius $R_0 = R_{\text{wd}} + \delta_{\text{BL}}$, where the size δ_{BL} of the BL is of the order of the stellar radius R_{wd} : $\delta_{\text{BL}} \propto R_{\text{wd}}$ (the BL is actually geometrically thick). The direct consequence of having an optically thin and geometrically thick BL is that the optically thick Keplerian disk will appear to have an inner hole of size δ_{BL} (possibly of the order of the radius of the WD R_{wd}). Two decades ago, it had already been pointed out that optically thin BL can explain the inner hole observed in circumstellar disks around young stellar objects (T Tauri stars, Godon (1996)). In other words, optically thin boundary layer are consistent not only with the X-ray data, but also with the UV data, as truncated optically thick disks produce a UV continuum with a shallow slope in better agreement with the UV observations than non-truncated disks.

It appears that the high mass accretion rate NL systems seem to systematically exhibit both optically thin hard X-ray emission and a UV continuum with a shallow slope that cannot be fitted with standard disk models, e.g. MV Lyr (Linnell et al. 2005; Balman et al. 2014), IX Vel (Long et al. 1994; Linnell et al. 2007), BZ Cam (Balman et al. 2014; Prinja et al. 2000), V592 Cas (Balman et al. 2014; Hoard et al. 2009), and RW Sex (Córdova et al. 1981; Linnell et al. 2010). Such a behavior indicates that this might be the rule for NL systems as a whole. We suspect that NLs, due to the optically thin BL, have a truncated inner disk with a radius of truncation $\approx 2R_{\text{wd}}$. Our recent *Swift* X-ray observations of the three NLs BZ Cam, MV Lyr, and V592 Cas (Balman et al. 2014) show optically thin boundary layers merged with advection-dominated accretion flows (ADAF) and/or hot coronae. In such systems, the BL energy is advected inwards as optically thin BLs cannot cool efficiently (Abramowicz et al. 1995). The

heating of the stellar surface can further result in an increased/inflated stellar radius.

Motivated by this, we decided to carry out an improved UV spectral analysis of the three NLs BZ Cam, MV Lyr, and V592 Cas, by modifying (truncating) the standard disk model. The three NL systems are reviewed in the next section together with their archival *FUSE* and *IUE* spectra. The modification of the standard disk model, presented in section 3, consists mainly in taking the inner radius of the optically thick disk to be at $R_0 = R_{\text{wd}} + \delta_{\text{BL}}$, where R_{wd} is the non-zero temperature WD radius and δ_{BL} is the size of the optically thin BL (which is now also a free parameter of size R_{wd} or smaller). We caution that *generating a standard disk model with an inner disk radius $R_0 > R_{\text{wd}}$ is not the same as truncating at R_0 a standard disk model generated with an inner disk radius at R_{wd}* , because the inner boundary condition is changed and, therefore, generates a new *mathematical* solution that has a lower temperature (although similar to the standard disk model, it is different). We briefly present the stellar spectral modeling in section 4, and show how the disk spectra are affected by our modification. In section 5, the results show that the modified disk model provides a better fit to the observed UV spectra of these three novalikes. In section 6, we check a possible correlation between the slope of the UV spectrum and the X-ray hardness ratio for a sample of CVs. We also discuss the possibility that the optically thin (truncated) inner region of the disk might be extended in the VY Scl subclass of NLs, and we also quantitatively check the departure of UV spectra from the standard disk model for disk-dominated CV subtypes. We present our conclusion in section 7.

2. THE THREE NOVALIKES MV LYR, BZ CAM, & V592 CAS

The three systems MV Lyr, BZ Cam, and V592 Cas were the three targets of our *Swift* X-ray observations (Balman et al. 2014), and while this might seem to be the main reason for choosing them for our UV spectral analysis, these systems have some characteristics that make them especially relevant for the kind of spectral analysis we are performing here. In order to demonstrate that some NL systems are best modeled with truncated disks, we choose systems in which the shallow slope of the UV flux continuum is incontrovertible. Namely, we want to ensure that the shallow slope is not due to an unknown reddening or to the wrong choice of system parameters such as the WD mass, radius, the distance to the system, or its inclination.

With a spectral coverage from $\sim 910\text{\AA}$ to $\sim 1190\text{\AA}$, *FUSE* covers the Lyman series and is therefore more useful in helping determine the hot component (WD temperature and/or mass accretion rate) of CVs than any other UV telescope. However, we wish to use the broadest spectral UV coverage possible, and we try to choose systems that have both *FUSE* and *IUE* spectra, thereby extending from the Lyman limit $\sim 910\text{\AA}$ to

the near ultraviolet $\sim 3,200\text{\AA}$. There are many hundreds (if not thousands) of known CVs, and almost 300 of them have good *IUE* spectra from $\sim 1150\text{\AA}$ to $\sim 3200\text{\AA}$. Usually the *IUE* spectra are easily used to derive the reddening ($E(B-V)$) toward the system using the 2175\AA feature (with an accuracy of about 25%, Fitzpatrick (1999)). Since it is not clear that one can use the same standard reddening law for all CVs in the Galaxy (e.g. Fitzpatrick (1999)), it would be preferable to choose systems with zero or negligibly small reddening $E(B-V) \approx 0$. In the present work we use the extinction curve from Fitzpatrick & Massa (2007) with $R=3.1$ to deredden the UV spectra.

Another desirable feature is the inclination of the systems. A high inclination system will be more affected by the orbital phase. In addition the standard disk model is a two dimensional flat disk and its departure from a three-dimensional realistic disk will be more pronounced at higher inclinations. We therefore prefer to choose systems with a small inclination.

When modeling the accretion disk, it is preferable to know the distance and/or WD mass to derive a more precise mass accretion rate (knowing only one of the two is most often good enough).

These conditions ensure that the failure of the standard disk model is not due to a wrong reddening (or reddening law), an unknown WD mass or distance. Although it has already been shown statistically that the failure of the standard disk model is due to the model itself, see Puebla et al. (2007).

Table 1. System Parameters

Parameter	MV Lyr	BZ Cam	V592 Cas
$M_{\text{wd}} < M_{\odot} >$	0.73-0.8 ^(1,2)	0.4-0.7 ^(7,8)	0.75 ⁽¹³⁾
$M_{2nd} < M_{\odot} >$	0.3 ⁽¹⁾	0.3-0.4 ⁽⁷⁾	0.21 ⁽¹³⁾
$i < \text{deg} >$	10 ± 3 ^(3,4,5)	$\sim 15 < 40$ ⁽⁹⁾	28 ± 10 ⁽¹⁴⁾
$E(B-V)$	0 ⁽⁶⁾	0.05 ⁽¹⁰⁾	0.22 ⁽¹³⁾
$P < \text{hr} >$	3.19 ⁽⁴⁾	3.69 ^(11,12)	2.76 ⁽¹⁵⁾
$d < \text{pc} >$	473 ± 37 ^(1,2)	830 ± 160 ⁽⁹⁾	$330-364$ ^(13,14)

NOTE—References: (1) Hoard et al. (2004); (2) Godon et al. (2012) (3) Schneider et al. (1981); (4) Skillman et al. (1995); (5) Linnell et al. (2005); (6) Bruch & Engel (1994); (7) Lu & Hutchings (1985); (8) Greiner et al. (2001); (9) Ringwald & Naylor (1998); (10) Prinja et al. (2000); (11) Patterson et al. (1996); (12) Honeycutt et al. (2013); (13) Hoard et al. (2009); (14) Huber et al. (1998); (15) Taylor et al. (1998)

We list the system parameters in Table 1, from which it appears that MV Lyr is possibly the best choice: it has no reddening, a very small inclination, and the distance, mass (and radius) and temperature of the WD have all been well determined. BZ Cam too is a very good choice,

but its WD mass is not known accurately. BZ Cam is known to exhibit an *IUE* spectrum that has a remarkably flat (see section 2.2) continuum slope, therefore presenting a challenging test to our modified disk model. As for V592 Cas, it has a large reddening value, but its parameters are otherwise relatively well known; its spectrum presents a UV continuum slope that is rather common for disk-dominated CVs (as discussed in Sec.6).

In the following subsections, we describe in detail these three systems and their archival UV spectra, providing also their important characteristics.

2.1. *MV Lyrae*

MV Lyr has an inclination $i \sim 10^\circ$ (Schneider et al. 1981; Skillman et al. 1995; Linnell et al. 2005), and zero reddening (Bruch & Engel 1994). It is a VY Scl nova-like system, i.e. spending most of its time in a high state and occasionally undergoing short-duration drops in brightness, or “low state”, when accretion is almost shut off and the WD is revealed in the UV. It has a distance $d \sim 500\text{pc}$ and a WD mass of $M_{\text{wd}} \sim 0.73 - 0.80M_\odot$ (Hoard et al. 2004; Linnell et al. 2005; Godon et al. 2012). Compared to other CVs, the values of these parameters are relatively well known. The orbital period of the binary is $P = 3.19\text{hr}$ and the mass ratio was found to be $q = M_{2\text{nd}}/M_{\text{wd}} = 0.4$ (Schneider et al. 1981; Skillman et al. 1995). The system parameters are listed in Table 1.

MV Lyr spends most of its time in the high state, at a visual magnitude of $\sim 12 - 13$, when the emission is primarily from the accretion disk. From time to time it drops into a low state, reaching a magnitude of ~ 17.5 , when the emission is possibly entirely from the WD. MV Lyr also has periods during which it is in an intermediate state at a magnitude of $\sim 14.-15$. MV Lyr was observed with *FUSE* and *IUE*, in a low state, with *IUE* in an in-

termediate state, and with *FUSE* and HST/STIS in a high state. The *IUE* observations of MV Lyr during its low state revealed a hot WD possibly reaching 50,000K (Szkody & Downes 1982) or higher (Chiappetti et al. 1982). These results were later confirmed with a *FUSE* spectroscopic analysis in a low state (Hoard et al. 2004), during which the mass accretion rate was estimated to be no more than $\dot{M} \approx 3 \times 10^{-13}M_\odot/\text{yr}$ and the WD temperature was found to be 47,000K. A follow-up analysis to study the different states of MV Lyr was carried out by Linnell et al. (2005) who found that standard disk models did not fit the observed spectra. Their models improved with the truncation of the inner disk, an isothermal radial temperature profile in the outer disk, or both, and gave a mass accretion rate of the order of $3 \times 10^{-9}M_\odot/\text{yr}$ for the high state and $1 \times 10^{-9}M_\odot/\text{yr}$ for the intermediate state.

The departure from the standard disk model is more pronounced in the intermediate state and most evident in the longer wavelengths of *IUE*. Since the high state was only observed down to $\sim 1,800\text{\AA}$, in our analysis we only model the system in the low and intermediate states extending above $3,000\text{\AA}$. The modeling of the low state is first carried out (see section 5.1) to demonstrate the numerical method and re-derive the system parameters. The observation log is recapitulated in Table 2. The spectra are shown in Fig.1 together with a standard disk model for comparison. The shallow slope of the *IUE* spectra in the intermediate state appears clearly.

All of the *FUSE* spectra in this work were calibrated with the latest and final version of CalFUSE (Dixon et al. 2007), and processed using our suite of FORTRAN programs, unix scripts, and IRAF procedures written for this purpose. The details can be found in Godon et al. (2012).

Table 2. Observation Log

System Name	Telescope/ Instrument	Obs ID	Date (UT) yyyy-mm-dd	Time (UT) hh:mm:ss	Exp. Time seconds	State l-i-h
MV Lyr	FUSE	C0410301	2002-07-07	11:56:39	11209	l
	IUE/SWP	07296	1979-12-02	20:09:28	5400	i
	IUE/LWP	06288	1979-12-02	18:52:24	4200	i
	IUE/SWP	10905	1980-12-27	11:29:05	2400	l
	IUE/SWP	10906	1980-12-27	13:18:44	9000	l
	IUE/LWP	09589	1980-12-27	12:12:51	3600	l
	IUE/LWP	09590	1980-12-27	15:50:09	7080	l
BZ Cam	FUSE	D9050101	2003-12-01	17:39:28	13187	h
	IUE/LWP	14485	1988-11-19	14:25:08	1500	h
	IUE/LWP	14486	1988-11-19	14:45:36	1500	h
	IUE/LWP	14487	1988-11-19	17:51:15	1500	h
	IUE/LWP	14491	1988-11-20	13:44:17	1500	h
	IUE/LWP	14492	1988-11-20	15:38:36	1380	h

Table 2 continued

Table 2 (*continued*)

System Name	Telescope/ Instrument	Obs ID	Date (UT) yyyy-mm-dd	Time (UT) hh:mm:ss	Exp. Time seconds	State l-i-h
V592 Cas	IUE/LWP	14493	1988-11-20	17:31:46	1380	h
	IUE/SWP	34775	1988-11-19	14:04:30	1800	h
	IUE/SWP	34776	1988-11-19	16:23:32	3600	h
	IUE/SWP	34777	1988-11-19	18:25:06	1440	h
	IUE/SWP	34784	1988-11-20	12:16:20	3600	h
	IUE/SWP	34785	1988-11-20	14:21:57	3600	h
	IUE/SWP	34786	1988-11-20	16:16:59	3600	h
	IUE/SWP	34787	1988-11-20	17:05:03	2520	h
	FUSE	D1140101	2003-08-05	21:22:24	23751	h
	IUE/LWP	12084	1981-12-05	19:48:23	1200	h
	IUE/LWP	12085	1981-12-05	22:24:02	1680	h
	IUE/SWP	15658	1981-12-05	18:48:15	900	h
	IUE/SWP	15659	1981-12-05	21:20:02	3600	h

NOTE—Note: (1) The flux level is h=high, i=intermediate, l=low.

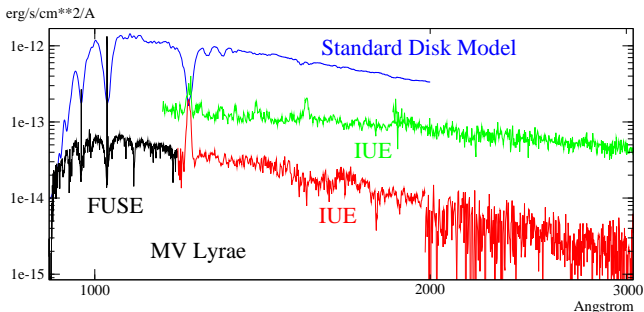


Figure 1. MV Lyrae has been observed in low, intermediate, and high states; however, only the low and intermediate states have IUE spectral coverage all the way to 3200Å. Shown here are the *FUSE* (black) and IUE (SWP+LWP) spectra of MV Lyr obtained in the low state (red), as well as an IUE (SWP+LWP) spectrum taken in an intermediate state (green). The low state reveals the WD, while the intermediate state is expected to be dominated by emission from the disk. However, the slope of the continuum of the spectrum obtained in the intermediate state is significantly shallower than the spectrum of a standard disk model, shown here in blue. The disk model has a central WD mass of $0.8M_{\odot}$, mass accretion rate of $10^{-8}M_{\odot}/\text{yr}$ and inclination of 41° . The disk spectrum has been shifted upwards for clarity as it is displayed only to show the slope of its continuum (there is no attempt here to fit the observed spectra with the theoretical disk spectrum). The observed spectra have not been shifted.

2.2. BZ Camelopardalis

BZ Cam is a VY Scl NL type (Garnavitch & Szkody 1988; Greiner et al. 2001), with a relatively small reddening $E(B-V)=0.05$ (Prinja et al. 2000), an orbital pe-

riod of 221min (Patterson et al. 1996), a distance of $830 \pm 160\text{pc}$ (Ringwald & Naylor 1998), and a moderately low inclination $\sim 12 < 40^{\circ}$ (Ringwald & Naylor 1998). Its WD mass is unknown but in our analysis we assume $M_{\text{wd}} \approx 0.4M_{\odot} \leq M_{\text{wd}} \leq 0.7M_{\odot}$ (Greiner et al. 2001). BZ Cam is not a typical CV in that it is surrounded by a faint emission bow-shock nebula (Ellis et al. 1984; Krautter et al. 1987; Greiner et al. 2001), which is proof of an outflow (Patterson et al. 1996). All the system parameters of BZ Cam are listed in Table 1 with their references.

BZ Cam spends most of its time in a high state at a magnitude of $\sim 12 - 13$. It has been shown to drop occasionally to a magnitude of ~ 14 . All the UV spectra of BZ Cam were collected in the high state, but show some small variations in the continuum flux level. The first Ultraviolet (UV) spectra of BZ Cam were obtained with *IUE* (Krautter et al. 1987; Woods et al. 1990, 1992; Griffith et al. 1995). We retrieved here 13 *IUE* spectra from a single epoch (1988-11-19 & 1988-11-20) with the same continuum flux level. They consist of 6 *IUE* LWP spectra and 7 *IUE* SWP spectra, which we co-added and then combined (see Table 2). The *IUE* (SWP & LWP) and optical continuum is consistent with a $\sim 12,500\text{K}$ Kurucz LTE model atmosphere with $\log g = 2.5$ (Prinja et al. 2000), but it cannot be attributed to the WD, because of its small emitting surface area. The *IUE* spectra of BZ Cam has a relatively shallow slope when compared to an accretion disk. BZ Cam also has a *FUSE* spectrum (Froning et al. 2012), which was never previously modeled with realistic disk or WD atmosphere model spectra. The *FUSE* spectrum is affected by interstellar (ISM) absorption, mainly molecular hydrogen. The *FUSE* and *IUE* spectra of BZ Cam

are shown (using a coarse binning for clarity) in Fig.2. together with a standard disk model and a 12,500K stellar atmosphere (with $\log g = 8$) spectrum for comparison. The continuum flux level in the *FUSE* spectrum is slightly lower than the continuum flux level of the combined *IUE* spectrum in the region where the two spectra overlap. This difference is likely due to a small variation in the flux of BZ Cam, although we cannot exclude the possibility that it could also be due, at least in part, to the fact that the data were obtained with different telescopes, gratings, detectors, and software.

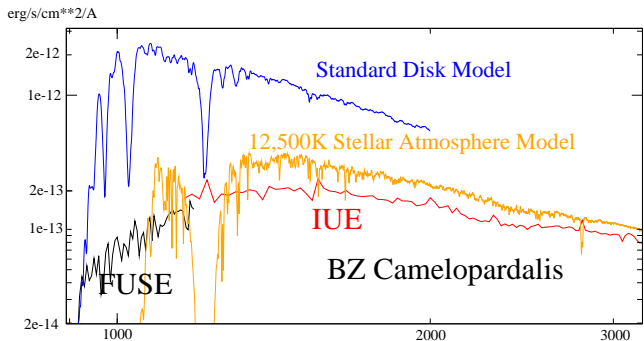


Figure 2. The dereddened *FUSE* (in black) and *IUE* (red) spectra of BZ Cam in its high state have been drawn on a log-log scale together with the theoretical spectra of a standard disk model (blue) and a 12,500K stellar atmosphere (orange) for comparison. The accretion disk has a WD mass of $0.8M_{\odot}$, mass accretion rate of $10^{-8}M_{\odot}/\text{yr}$ and inclination $i = 18^{\circ}$. The theoretical spectra have been shifted upwards for clarity. We do not attempt here to “fit” the theoretical spectra to the observed ones. The relatively shallow slope of the *IUE* spectrum does not match the steeper slope of a standard accretion disk, and is even more shallow than the 12,500K isothermal component. On this log-scaled figure, it appears that the *IUE* spectrum does not especially match the *FUSE* spectrum both in its continuum flux level and slope. The observed spectra were not obtained at the same time, and since BZ Cam is a variable UV source, the spectra cannot be combined together for modeling. In this figure, the *FUSE* and *IUE* spectra have been binned coarsely for clarity.

2.3. *V592 Cassiopeiae*

V592 Cas is an UX UMa subtype of novalike and has never been observed in a low brightness state. It has an inclination of $i = 28^{\circ}$, a mass ratio of 0.19 (Huber et al. 1998), and its orbital period is $P_{\text{orb}} = 2.76$ hr (Taylor et al. 1998; Witherick et al. 2003). It shows evidence for a bipolar wind outflow (Witherick et al. 2003; Kafka et al. 2009; Prinja et al. 2004) with velocities reaching up to $v_{\text{wind}} \sim 5000$ km s^{-1} (Kafka et al. 2009). The reddening toward the system is $E(B-V) = 0.22$ (Cardelli et al. 1989), and its distance is about 240-360 pc (Taylor et al. 1998). The mass accretion

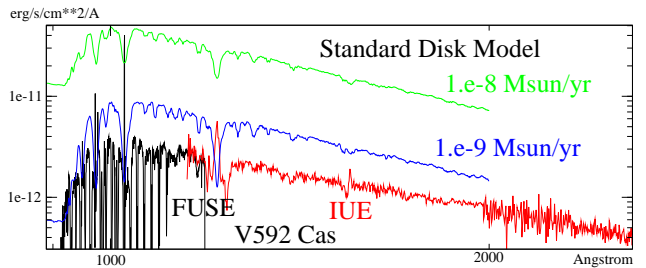


Figure 3. The dereddened *FUSE* (solid black) and *IUE* (red) spectra of *V592 Cas* in its normal high state have been plotted on a log-log scale against two standard disk model spectra for comparison. The theoretical spectra have been shifted upward for clarity, there is no attempt here to “fit” the observed spectra with the theoretical ones. The standard disk models have a central WD mass of $0.8M_{\odot}$ with mass accretion rate of $\dot{M} = 10^{-8}M_{\odot}/\text{yr}$ (green/upper plot) and $\dot{M} = 10^{-9}M_{\odot}/\text{yr}$ (blue/lower plot), and inclination of 41° and 18° respectively. The *FUSE* flux continuum shape is in better agreement with the $10^{-8}M_{\odot}/\text{yr}$ model at wavelengths shorter than $1,000\text{\AA}$, while the *IUE* flux continuum slope is even shallower than the $10^{-9}M_{\odot}/\text{yr}$ model. These are clear indications that the spectra do not agree with the standard disk model. The *FUSE* spectrum is strongly affected by molecular hydrogen absorption lines from the interstellar medium (ISM).

rate of the system is believed to be of the order of $\approx 1 \times 10^{-8}M_{\odot}/\text{yr}$ (Taylor et al. 1998; Hoard et al. 2009). In the present work, we assume the WD to have a standard CV WD mass of $\sim 0.8M_{\odot}$ and a temperature of 45,000K (Hoard et al. 2009).

V592 Cas was observed with *IUE* on December 5th 1981. We retrieved the two LWR spectra and two of the four SWP spectra that were obtained, combined and co-added them to generate a spectrum with a spectral range from $\sim 1150 \text{\AA}$ to $\sim 3,200 \text{\AA}$. With a flux of a few $10^{-13}\text{erg/s/cm}^2/\text{\AA}$, the spectrum has a relatively good signal in the SWP segment but it is rather noisy in the LWR segment, as shown in Fig.3 (in red). *V592 Cas* has 3 *FUSE* data sets, obtained on August 5, 7 and 8, 2003. The data sets have all the same quality and about the same exposure time and reveal the same spectrum. We decided to retrieve the first data set (D1140101) and extracted a final spectrum following the same procedure we used for BZ Cam and MV Lyr. The *FUSE* spectrum *V592 Cas* has the same continuum flux level as the *IUE* spectrum in the region where the two spectra overlap. Like the *FUSE* spectrum of BZ Cam, the *FUSE* spectrum of *V592 Cas* is heavily affected by ISM molecular hydrogen lines, appearing in Fig.3 (in black) as if the spectrum had literally been sliced.

In Fig.3 we also plot two standard disk models for comparison. The *FUSE* continuum is in better agreement with the $10^{-8}M_{\odot}/\text{yr}$ model, while the *IUE* continuum slope is even shallower than the $10^{-9}M_{\odot}/\text{yr}$ model. These indicates that the combined *FUSE* + *IUE* spectrum does not agree very well with the standard disk model. However, the discrepancy is not as strong as for MV Lyr and BZ Cam.

3. THE MODIFIED DISK MODEL

We wish to model the three NL systems in high and intermediate states using a disk model generated by modifying the standard disk model. Therefore, we first review the standard disk model, and then we introduce the modification we make.

3.1. The Standard Disk Model

In the standard disk theory (Pringle 1981), the total accretion luminosity that can be released by accretion onto a star is given by:

$$L_{\text{acc}} = \frac{GM_{\text{wd}}\dot{M}}{R_{\text{wd}}}, \quad (1)$$

where G is the gravitational constant, \dot{M} the mass accretion rate, M_{wd} the mass of the accreting star (here a WD) and R_{wd} its radius.

In disk systems, accretion energy is released through the disk. All the current disk models are based on the Shakura-Sunyaev ‘alpha’ disk model known as the *standard disk model* (Shakura & Sunyaev 1973; Lynden-Bell & Pringle 1974). The disk is assumed to be geometrically thin (in the vertical dimension) and the energy dissipated between adjacent rings of matter (Φ_{ν} , the dissipation function due to the shear) is radiated locally in the vertical direction: $\sigma T_{\text{eff}}^4 = \Phi_{\nu}$. The viscosity ν is due to turbulence and has been shown to come from a magneto-rotational instability (Balbus & Hawley 1991). The turbulent viscosity is parametrized with an *a priori* unknown parameter α ($\alpha < 1$), which is the reason the standard disk model is also called the alpha disk model. The standard disk model is obtained from the steady-state Navier-Stokes equations in cylindrical coordinates (R, ϕ, z). The equations are reduced to one dimension (R) after integrating in the vertical dimension (z), and assuming axi-symmetry ($\partial\phi/\partial = 0$). Using the conservations of mass (for \dot{M}) and angular momentum, and imposing the boundary condition that the angular velocity gradient vanishes ($\partial\Omega/\partial R = 0$) at the inner boundary $R = R_{\text{wd}}$, one obtains the standard disk model Pringle (1981). In that approximation the boundary layer between the star and disk is geometrically thin, its thickness can be neglected $\delta_{\text{BL}} \ll R_{\text{wd}}$.

3.2. The New Boundary Condition

We modify the standard disk model by truncating the inner disk at a radius $R_0 > R_{\text{wd}}$. In order to do this correctly, one cannot just remove the inner disk between R_{wd} and R_0 from a standard disk model starting at R_{wd} , instead one has to generate a standard disk model starting at $R = R_0$. We give here below, several reasons for having a disk starting at R_0 rather than R_{wd} .

The optically thin boundary layer simulations of Narayan & Popham (1993) and Popham (1999) show that the optically thin boundary layer has a size $\delta_{\text{BL}} \approx R_{\text{wd}}$ and that the angular velocity gradient vanishes at the outer edge of the boundary layer. Namely, the no-

shear boundary condition $\partial\Omega/\partial R = 0$ has to be imposed at $R = R_0 = R_{\text{wd}} + \delta_{\text{BL}} > R_{\text{wd}}$.

If the inner hole in the disk is due to a weakly magnetized WD truncating the disk (Hameury & Lasota 2002) at R_0 (as in intermediate polars - IPs), one still has the same new boundary conditions, as R_0 is now the corotation radius, which by definition is the radius where $\partial\Omega/\partial R = 0$, since $\Omega = \text{constant}$ there.

If the inner hole in the disk is due to evaporation (Hameury et al. 2000), the same new boundary conditions can also be imposed as the disk only starts at the outer radius (now R_0) of the evaporated inner disk.

Also, it is important to note that the radius of the WD is expected to increase as the WD temperature increases. For example a 10,000K WD of mass $0.7M_{\odot}$ has a radius $R_{\text{wd}} = 7.9 \times 10^8 \text{cm}$, and at 50,000K the radius increases by 16% to $R_{\text{wd}} = 9.2 \times 10^8 \text{cm}$ (Wood 1995). The increase in radius is even more pronounced for a smaller mass WD and basically reaches a factor of 2 for a $0.4M_{\odot}$ WD, with a zero-temperature radius of $R_{\text{wd}} = 1.1 \times 10^9 \text{cm}$ versus a 50,000K radius of $R_{\text{wd}} = 2 \times 10^9 \text{cm}$ (Wood 1995). Since the VY Scl systems are notorious for having a temperature much hotter than other CVs at the same period, the change in radius cannot be ignored. So far, most standard disk model spectra were computed assuming a constant (zero-temperature) radius (Wade & Hubeny 1998; Godon et al. 2012), thereby not taking into account the increased WD radius and possibly overestimating the disk temperature. Modeling the disk properly requires that the WD temperature be known, and requires a fine tuning of the modeling such as the one performed in Linnell et al. (2008).

The modified disk model can therefore be applied to different inner disk structures, including the magnetically truncated disks in IP systems, and around hot CV WDs to provide a more realistic approach for the modeling of the disk.

3.3. The Temperature of the Modified Disk

Our modified disk model differs from the standard disk model in that we now impose the no-shear boundary condition at $r = R_0 > R_{\text{wd}}$. Namely,

$$\frac{\partial\Omega}{\partial R} = 0, \quad R = R_0, \quad (2)$$

and, following Pringle (1981), we assume a Keplerian velocity $\Omega = \Omega_K$ for $R \geq R_0$.

With these assumptions and boundary conditions one obtains the disk radial temperature profile

$$T_{\text{eff}}(R) = \left\{ \frac{3GM_{\text{wd}}\dot{M}}{8\pi\sigma R^3} \left[1 - \sqrt{\frac{R_0}{R}} \right] \right\}^{1/4}, \quad (3)$$

where the angular velocity in the disk has been substituted with its Keplerian value. For convenience, this expression can be written as

$$T_{\text{eff}}(x) = T_0 x^{-3/4} (1 - x^{-1/2})^{1/4}, \quad (4)$$

with

$$T_0 = 64,800K \times \left[\left(\frac{M_{\text{wd}}}{1M_{\odot}} \right) \left(\frac{\dot{M}}{10^{-9}M_{\odot}/\text{yr}} \right) \left(\frac{R_0}{10^9\text{cm}} \right)^{-3} \right]^{1/4} \quad (5)$$

where $x = R/R_0$. This model gives a maximum temperature ($T_{\text{max}} = 0.488T_0$) at $x = 1.36$, and $T = 0K$ at $R = R_0$ ($x = 1$).

The expression for the temperature of the modified disk model is the same as for the standard disk model, except for the star radius R_{wd} , which has simply been replaced by the inner disk radius R_0 . For example, for an inner disk radius twice as large as the star radius ($R_0 = 2R_{\text{wd}}$), the maximum effective surface temperature in the disk (reached at $R = 1.36R_0$) has dropped to $\sim 65\%$ the value it has in the standard disk model (at $R = 1.36R_{\text{wd}}$). In Fig.4 we show the temperature profile for a modified disk model for different value of the truncated radius R_0 . The mass of the WD is $0.8M_{\odot}$, and the mass accretion rate is $1 \times 10^{-9}M_{\odot}/\text{yr}$. The radius R_0 is given in units of the WD radius R_{wd} (which is itself obtained from the WD mass-radius relation, e.g. Wood (1995)). From Fig.4, it is clearly apparent that truncating a standard disk model by solely removing the region $R < 2R_{\text{wd}}$ gives a disk model with a much higher temperature in the inner disk than generating a model starting at $R_0 = 2R_{\text{wd}}$. As the size of the BL is possibly not negligible and as the WD can easily increase its radius with increasing temperature, the standard disk model can over-estimate the temperature in the inner disk by a large fraction.

While our modified disk model is actually a standard disk model in which the radius of the star R_{wd} has been replaced by the inner radius of the disk R_0 (where $R_0 > R_{\text{wd}}$), we use through this paper the terms *modified disk* and *standard disk* to differentiate between the two.

3.4. The Luminosity of the Modified Disk

The disk luminosity L_{disk} is given by integrating Φ_{ν} (or σT_{eff}^4) over the surface of the disk

$$L_{\text{disk}} = 2 \int_{R_0}^{\infty} \Phi_{\nu} 2\pi R dR = \frac{1}{2} \frac{GM_{\text{wd}}\dot{M}}{R_0}. \quad (6)$$

In the standard disk model the disk luminosity amounts to half the accretion energy, in the modified disk model it is smaller than half the accretion energy. For example, for $R_0 = 2R_{\text{wd}}$ the disk luminosity is only half the disk luminosity expected for a standard non-truncated disk. **The important point is that a truncated disk cannot be generated by simply truncating a standard disk model, but it has to be obtained as a standard disk model in which R_{wd} is replaced by R_0 , which produces a much lower disk temperature and luminosity.** The idea of replacing R_{wd} by R_0 was discussed briefly in the modeling of IX Vel (Long et al. 1994) but was never followed through. Similarly the modeling of MV Lyr by Linnell et al. (2005)

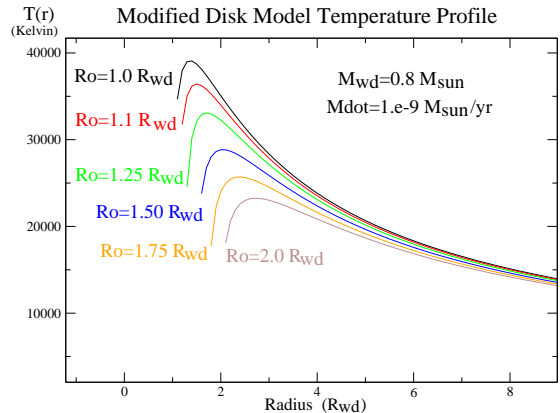


Figure 4. The temperature profile of the modified disk model is shown as the radius R_0 (in units of R_{wd}) of the inner boundary of the disk is increased from one stellar radius (the standard disk model) to two stellar radii. Here the WD mass is $0.8M_{\odot}$ and the mass accretion rate is $\dot{M} = 1 \times 10^{-9}M_{\odot}/\text{yr}$. As R_0 increases, the disk temperature profile flattens and the disk luminosity decreases. For low M_{wd} and \dot{M} and for large R_0 , the temperature becomes almost isothermal.

includes a truncated disk, but with the ‘usual’ temperature profile of the standard disk model (R_{wd} was not replaced by R_0 , instead the standard disk was just truncated).

3.5. The Boundary Layer Luminosity

The remaining fraction of the accretion energy is dissipated at the inner edge of the disk, where the disk meets the surface of the star ($r = R_{\text{wd}}$), in the so-called boundary layer (BL). The fast (Keplerian) rotating ($\Omega_K(R_0)$) matter adjusts itself to the slowly rotating stellar surface (Ω_{wd}) and dissipates its remaining kinetic energy. The luminosity of the boundary layer L_{BL} , in the standard disk model, is of the same order of magnitude as $L_{\text{acc}}/2$, though usually smaller as some of the energy goes into spinning up the WD (Kluźniak 1987). This is true for optically thick boundary layers.

X-ray observations of disk-dominated CVs (e.g. van Teeseling et al. (1996); Balman et al. (2014)) show that the BL is optically thin and that the X-ray luminosity is much smaller than the disk luminosity, the BL is underluminous. For the optically thin boundary layer, one can only refer to the work of Narayan & Popham (1993); Popham (1999) and to observations.

3.6. The Fate of the Remaining Accretion Energy

If the disk emits less than half the accretion energy, and the boundary layer luminosity (in the X-ray) is itself only a fraction of the disk luminosity, one might ask where does the remaining energy go? When an accretion flow cannot cool efficiently, due to being optically thin, the energy is advected with the flow into the outer layer of the star (Abramowicz et al. 1995). The advected BL energy will then increase the WD temperature, and will likely drive an outflow as in Advection Dominated Accretion Flows - ADAF (Narayan & Yi 1995). This is sup-

ported by three observational facts: (i) The WD temperature of NLs is rather elevated when compared to other CVs with the same period. (ii) Many NL systems exhibit hot, fast wind outflows seen in P Cygni line structure and blue-shifted absorption. These winds originate in the inner disk/BL region but their source of energy has not yet been identified. Some CV systems even have visible ejected nebular material (e.g. BZ Cam, Ellis et al. (1984)). (iii) Recent X-ray observations of NLs (Balman et al. 2014) suggest that high-state NLs may have optically thin BLs merged with ADAF-like flows and/or hot coronae. Balman et al. (2014) showed that the observed discrepancy between the X-ray/boundary layer and disk luminosity can be accounted for if the boundary layer energy is heating the WD through advection ($T_{\text{wd}} \sim 50,000\text{K}$) and is also used to drive the wind outflows. The efficiency of the boundary layer to radiate its energy is then greatly reduced (< 0.01), consistent with the observed ratio of the X-ray to the disk UV-Optical luminosities.

For this reason, we expect NLs to be modeled with the modified disk model and the addition of a hot WD, itself possibly with an inflated radius.

3.7. The Outer Disk Modeling

In CVs the accreting WD is the more massive component and the Roche lobe radius is always larger than half the binary separation, i.e. $> a/2$. Due to the impact of the stream (from the first Lagrange point L1) on the rim of the disk and due to tidal interaction, the outer disk is expected to have a temperature larger than dictated by both the standard and modified disk models (Buat-Ménard et al. 2001). We assume here that the outer region of the disk has a temperature of 10,000K to 12,000K. We note that such a practice is not uncommon, and some authors (e.g. Linnell et al. 2005) have considered disk models with an elevated temperature ($\sim 10 - 12,000\text{K}$) in the outer region of the disk.

4. UV SPECTRAL MODELING

4.1. TLUSTY and SYNSPEC Codes

We use the FORTRAN suite of codes TLUSTY, SYNSPEC, ROTIN and DISKSYN (Hubeny 1988; Hubeny et al. 1994; Hubeny & Lanz 1995) to generate synthetic spectra of stellar atmospheres and disks. The codes include the treatment of hydrogen quasi-molecular satellite lines (low temperature) and LTE and NLTE options (high temperature). SYNSPEC generates a continuum with absorption lines. In the present case we do not generate emission lines. For disk spectra we use solar abundances and for stellar spectra we vary the abundances as needed. An introductory guide, a reference manual and an operational manual to TLUSTY and SYNSPEC have just been released and are available for full details of the codes (Hubeny & Lanz 2017a,b,c).

4.2. WD stellar atmosphere models

The code TLUSTY is first run to generate a one-dimensional (vertical) stellar atmosphere structure for a given surface gravity, effective temperature and surface composition of the star. Computing a single model is an iterative process that needs to converge. In the present case, we treat hydrogen and helium explicitly, and treat nitrogen, carbon and oxygen implicitly (Hubeny & Lanz 1995).

The code SYNSPEC is then run, using the output stellar atmosphere model from TLUSTY as an input, and generates a synthetic stellar spectrum over a given (input) wavelength range (it has capabilities to cover a spectral range from below 900Å and into the optical). The code SYNSPEC derives the detailed radiation and flux distribution of continuum and lines and generates the output spectrum (Hubeny & Lanz 1995). SYNSPEC has its own chemical abundances input to generate lines for the chosen species. For temperatures above 35,000K the approximate NLTE treatment of lines is turned on in SYNSPEC.

Rotational and instrumental broadening as well as limb darkening are then reproduced using the routine ROTIN. In this manner we have already generated a grid of WD synthetic spectra covering a wide range of temperatures and gravities with solar composition (see <http://synspecat.weebly.com/>).

4.3. Disk Models

The disk spectra are generated by dividing the disk into rings, each with a given radius r_i and temperature ($T(r_i)$), density and effective vertical gravity obtained from the modified disk model for a given stellar mass, inner and outer disk radii, and mass accretion rate.

The code TLUSTY generates a one-dimensional vertical structure for each disk ring. The input parameters are the mass accretion rate, the mass of the accreting star, the radius of the star, and the radius of the ring. The radius of the star in our modified disk model is set to be the inner radius of the disk R_0 .

SYNSPEC is then used to create a spectrum for each ring, and the resulting ring spectra are integrated into a disk spectrum using the code DISKSYN, which includes the effects of (Keplerian) rotational broadening, inclination, and limb darkening.

For disk rings below 10,000 K, we use Kurucz stellar spectra of appropriate temperature and surface gravity.

In Fig.5 we present the synthetic spectra of two disks generated with the suite of codes: a standard disk model (in black) and a modified disk model (in red). Both models have a $0.55M_{\odot}$ WD accreting at a rate of $\dot{M} = 10^{-9}M_{\odot}/\text{yr}$, and are displayed for an inclination $i = 40^{\circ}$. The standard disk has an inner radius at $R_0 = R_{\text{wd}}$, while the modified disk has an inner radius at $R_0 = 2R_{\text{wd}}$. The slope of the continuum of the modified disk is almost flat.

5. RESULTS

5.1. MV Lyrae

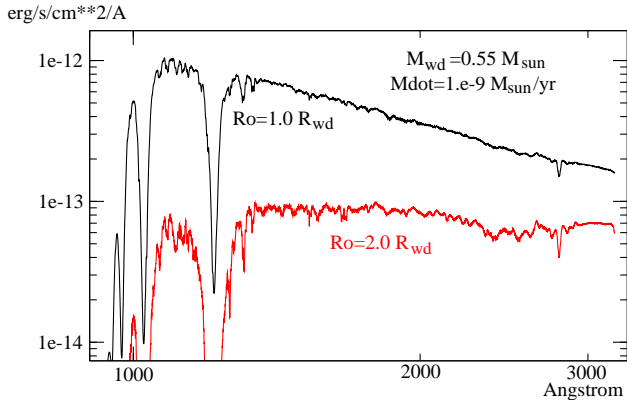


Figure 5. The synthetic spectra of two accretion disks are shown in the ultraviolet range. Both disk models have a $0.55M_{\odot}$ WD accreting at a rate of $10^{-9}M_{\odot}/\text{yr}$. The upper spectrum (in black) is a standard disk model with the inner disk radius at $R_0 = R_{\text{wd}}$, the lower spectrum (in red) is that of a modified disk with the inner radius at $R_0 = 2R_{\text{wd}}$. Because of the change in the disk temperature profile, the lower spectrum is characterized by a continuum slope that appears almost flat on this log-log scale. The continuum exhibits an “elbow” at $\lambda \sim 2400\text{\AA}$, which is a real feature observed in the *IUE* spectrum of BZ Cam.

The Low State— The modeling of the *FUSE* spectrum of MV Lyr in the low state was presented elsewhere (Godon et al. 2012) and gives identical results to the modeling of the combined *FUSE* + *IUE* spectrum presented here, which covers a much larger wavelength range. However, it is important to re-derive and confirm the distance to MV Lyr, its WD mass, radius, temperature and rotational velocity, because these are important parameters serving as input for the modeling of the intermediate state. Namely, these parameters are used as constraints in the modeling of the combined *FUSE* + *IUE* spectrum of MV Lyr in the intermediate state.

While the *FUSE* spectrum presents many absorption lines commonly detected in the atmosphere of accreting WDs (see Godon et al. (2012) for details), the *IUE* (SWP+LWP) spectrum is more noisy and presents only a continuum, in which the only identified absorption feature is the C IV 1550 line. The *FUSE* and *IUE* spectra match in their flux level and slope, in spite of the fact that they were obtained with different telescopes more than 20 years apart. This is possibly a sign that MV Lyr had reached a similar (if not identical) low state in which the WD completely dominates the FUV (Hoard et al. 2004).

Our fitting results yield (Godon et al. 2012): a WD temperature $T_{\text{wd}} = 44 - 47,000$ K, with a projected stellar rotational velocity $V_{\text{rot}} \sin i = 150 - 250$ km/s, chemical abundances $Z = 0.1 - 1.0Z_{\odot}$, and stellar surface gravity $\log g = 8.06 - 8.28$ ($M_{\text{wd}} = 0.7 - 0.8M_{\odot}$ with $R_{\text{wd}} = 9,010 - 7,450$ km). The resulting distance we obtained is ~ 464 pc for a $0.8M_{\odot}$ WD and ~ 560 pc for a $0.7M_{\odot}$ WD. In Fig. 6 we present a 45,000K WD fit as one of the solutions we obtained. The remarkable characteristic of this model fit is that, although it was originally

generated to fit the *FUSE* spectrum alone (Godon et al. 2012), as shown in Fig. 6, it actually also fits the *IUE* spectrum all way to the longest wavelengths $\sim 3000\text{\AA}$ (see Fig. 7; the region beyond 3000\AA is very noisy and has been discarded). From this fit one obtains relatively accurate values for some of the important system parameters.

These values of the parameters are consistent with the analysis of Hoard et al. (2004) who obtained $T_{\text{wd}} = 47,000$ K with $\log g = 8.25$ for a non-rotating WD, and $T_{\text{wd}} = 44,000$ K with $\log g = 8.22$ for a WD rotating at 200 km/s with elemental abundances of C=0.5, N=0.5 and Si=0.2 (solar), and a derived distance of 505 ± 50 pc.

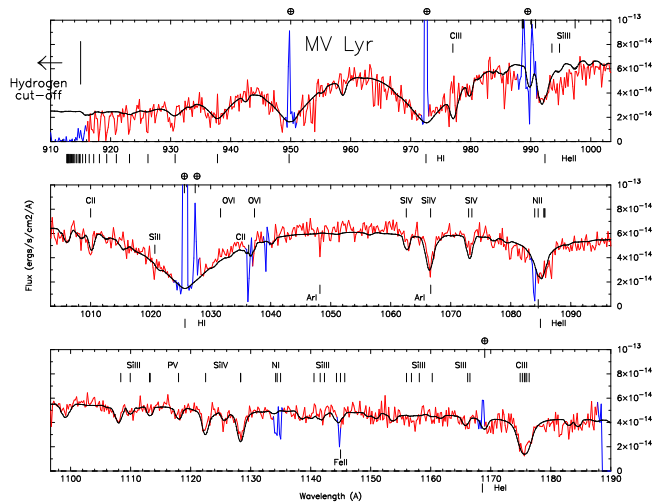


Figure 6. A synthetic WD atmosphere spectrum fit (in black) to the combined *FUSE* + *IUE* spectrum of MV Lyr (in red) in the low state (the blue shows the contamination by terrestrial airglow). This figure shows the *FUSE* range, while the next figures show the *IUE* range. The sharp emission lines are artifacts due to air glow (marked with a plus sign inside a circle at the top of each panel) or indirect reflection of sunlight inside the telescope (such as e.g. the He II 1168 \AA). The WD model has a temperature of $T_{\text{wd}} = 45,000$ K, solar composition and a projected rotational velocity of $V_{\text{rot}} \sin(i) = 200$ km/s.

The Intermediate State— MV Lyr was caught in an intermediate state with *IUE*, covering that region of the spectrum where the continuum slope departs strongly from a standard disk model all the way to $\sim 3,200\text{\AA}$. In order to model the intermediate state spectrum, we use the parameters we derived from fitting the low state: we adopt a WD mass of $M_{\text{wd}} = 0.73M_{\odot}$, with a temperature of $\sim 45,000$ K, a radius $R_{\text{wd}} = 8,500$ km and a distance of ~ 500 pc. We use the system inclination $i = 10^{\circ}$ from the literature (see Table 1).

We first attempt to fit the combined *IUE* SWP+LWP spectrum with a standard disk model, where the only varying parameter is the mass accretion rate (since the inclination and WD mass are fixed). The inner disk radius is simply R_{wd} and the outer radius of the disk is

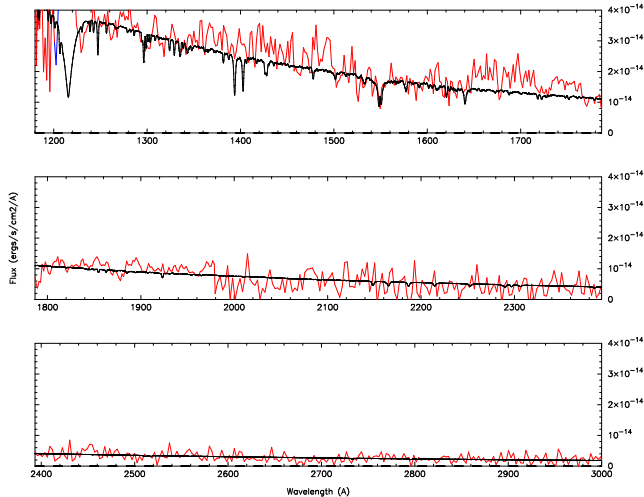


Figure 7. The synthetic WD atmosphere spectrum fit (in black) to the combined *FUSE* + *IUE* spectrum (in red) of MV Lyr in the low state is presented here showing only the *IUE* range. Note that the vertical scale is different than in Fig.6 for clarity.

place at a distance $a/3$, where a is the binary separation. Using the system parameters we have $a/3 \sim 30R_{\text{wd}}$. We also include the expected contribution of the 45,000K WD. In order to fit the distance to the system (by scaling the theoretical spectrum to the observed one), we find a mass accretion rate of $8 \times 10^{-10} M_{\odot}/\text{yr}$. However, this model does not fit the observed spectrum at all (see Fig.8), the theoretical spectrum is too “blue” when compared to the observed spectrum, consistent with the statistical analysis of Puebla et al. (2007).

Next, we fit the observed spectrum with modified standard disk models. For each given mass accretion rate we built disks with an increasing larger inner radius $R_0/R_{\text{wd}} = 1.0, 1.2, 1.5, 1.7, 2.0, 2.5$ and 3.0 . We kept the outer disk radius at $30R_{\text{wd}}$ and set the outer disk at a temperature around 10, 11 or 12,000K. The width of this isothermal outer disk region was also varied from $1R_{\text{wd}}$ to $10R_{\text{wd}}$ (i.e. to a maximum of $1/3$ of the disk radial extent). The increase in the inner disk radius, produces a decrease of flux more pronounced in the shorter wavelength region of the spectrum, while the setting of the outer isothermal disk region produces a relative increase of flux in the longer wavelength region. We find that a best fit is obtained for a mass accretion rate of $2.4 \times 10^{-9} M_{\odot}/\text{yr}$ with an inner hole of size $2.0R_{\text{wd}}$ and an outer disk, from $20R_{\text{wd}}$ to $30R_{\text{wd}}$, set with a temperature of 10,000K. This model is presented in Fig.9 and also includes the contribution of 45,000K WD. The strong emission lines are shown in blue, there are more emission lines on the edges of the $\text{Ly}\alpha$ profile which we are not modeling, as they form in an optically thin medium. The fit to the continuum is much

improved, when compared to the standard disk model.

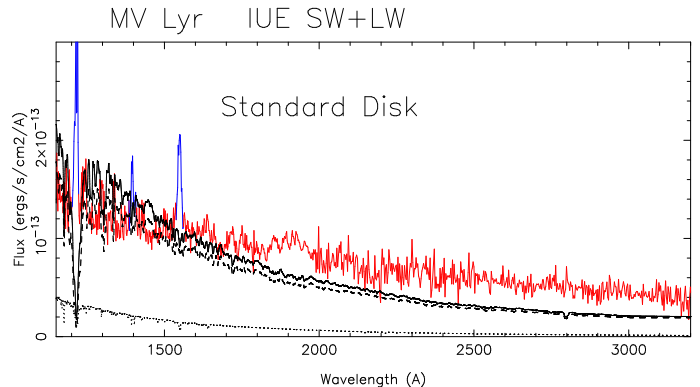


Figure 8. The combined SWP + LWP *IUE* spectrum of MV Lyra in an intermediate state (solid red line; strong emission lines in blue) is modeled with a hot WD (45,000K) and a standard accretion disk with $\dot{M} = 8 \times 10^{-10} M_{\odot}/\text{yr}$ and $i = 10^\circ$. The inner radius of the disk is at $1R_{\text{wd}}$ and the outer radius is at $30R_{\text{wd}}$. The combined model WD+disk is the solid black line, the dotted line in the lower part of the panel shows the WD contribution, the dashed line shows the contribution from the disk. The model cannot match the continuum flux level, it is far too ‘blue’.

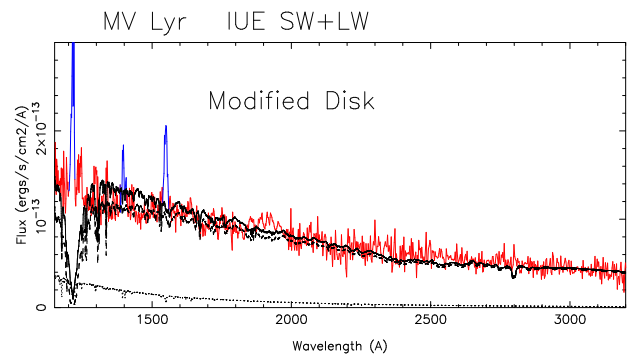


Figure 9. The same *IUE* spectrum (in red) as in Fig.8 is modeled here with a hot WD (dotted line) and our modified disk model (dashed line); the combined model is the solid black line. The mass accretion rate is $\dot{M} = 2.4 \times 10^{-9} M_{\odot}/\text{yr}$ and $i = 10^\circ$. The inner edge of the disk is placed at $R_0 = 2.0R_{\text{wd}}$. The outer region ($20R_{\text{wd}}$ to $30R_{\text{wd}}$) of the disk has been set at a temperature of 10,000K. The strong emission lines are shown in blue, there are more emission lines on the edges of the $\text{Ly}\alpha$ profile which we are not modeling, as they form in an optically thin medium.

5.2. *BZ Camelopardalis*

BZ Cam has a *FUSE* spectrum and an *IUE* spectrum that do not have exactly the same flux level, in addition the *IUE* spectrum is consistent with a rather cold component, while the *FUSE* spectrum seems to be consistent with a hotter component. Consequently, we first model these two spectra separately, and next we try to model the two spectra in a self-consistent manner.

Modeling the FUSE Spectrum— The *FUSE* spectrum shows the presence of a hot component contributing flux all the way to the shortest wavelengths of *FUSE*. We try a standard disk model, assuming $M_{\text{wd}} = 0.8M_{\odot}$, and we find that the mass accretion rate has to be as large as $10^{-8}M_{\odot}/\text{yr}$ to produce the observed flux in the short wavelengths of *FUSE*. This model, however, gives a distance of more than 2kpc, i.e. more than twice the accepted distance to the system. As we decrease the WD mass to $0.55M_{\odot}$, the distance decreases slightly to 1.8kpc, and for a $0.35M_{\odot}$ WD the distance is still too large, however, the flux in the shorter wavelengths of the theoretical spectrum is now too low. For a slightly lower mass accretion rate of $10^{-8.5}M_{\odot}/\text{yr}$, only the larger WD model with $M_{\text{wd}} = 0.8M_{\odot}$ provides enough flux in the short wavelengths, but here too the distance is too large and reaches 1.4kpc.

These results show that the single disk model does not provide a satisfactory fit. Since our modified disk model provides colder disks, we do not try to use such a modeling for the *FUSE* spectrum, as it would not provide enough flux in the shorter wavelengths.

Instead, we try single WD models. The best fit WD model has $M_{\text{wd}} = 0.4M_{\odot}$, $T_{\text{wd}} = 45,000\text{K}$, solar composition and $V_{\text{rot}} \sin(i) = 200\text{km/s}$, and the distance obtained from the fit is 791pc, when the WD radius is set to $R_{\text{wd}} = 18,540\text{km}$. This model is shown in Fig.10, and includes a basic modeling of the ISM molecular hydrogen absorption lines (see Godon et al. (2007) for details). In the short wavelengths ($\sim 960\text{\AA}$ upper panel) the model has too much flux, while in the longer wavelengths (lower panel) the model has too little flux. A 40,000K WD gives a distance of 654pc while a 50,000K WD gives a distance of 933pc. We note that at a temperature of about 50,000 K the radius of the $0.4M_{\odot}$ WD model ($\sim 2 \times 10^9\text{cm}$) is about twice that of the zero-temperature model ($\sim 1 \times 10^9\text{cm}$).

Next, we increase the WD mass to $0.7M_{\odot}$, and accordingly decrease the radius to $\sim 0.9 \times 10^9\text{cm}$, we find that the scaled distance from the fit becomes too short for the same temperature, and higher temperature models ($T > 50,000\text{K}$) do not provide the best fit. The fit of the 45,000K $0.7M_{\odot}$ WD is as good as the $0.4M_{\odot}$ fit with the same temperature, and indicates that a $0.7M_{\odot}$ WD with a radius of $\sim 2 \times 10^9\text{cm}$ provides a valid solution indicating that maybe the radius of the WD is inflated.

We also try to add a standard disk model to the WD disk model, but we find that disk model deteriorates the fit and increases the distance well above 1kpc.

To summarize, the *FUSE* spectrum of BZ Cam is best fitted with a single WD with a temperature of 45,000K $\pm 5,000\text{K}$, and a mass $0.4 - 0.7M_{\odot}$ (from the literature) as long as the WD radius is $\sim 2 \times 10^9\text{cm}$ (to fit the known distance to the system). Since this radius really corresponds to a $0.4M_{\odot}$ WD at $T \sim 50,000\text{K}$ (see section 3.2), this is the WD mass we adopt as the best solution.

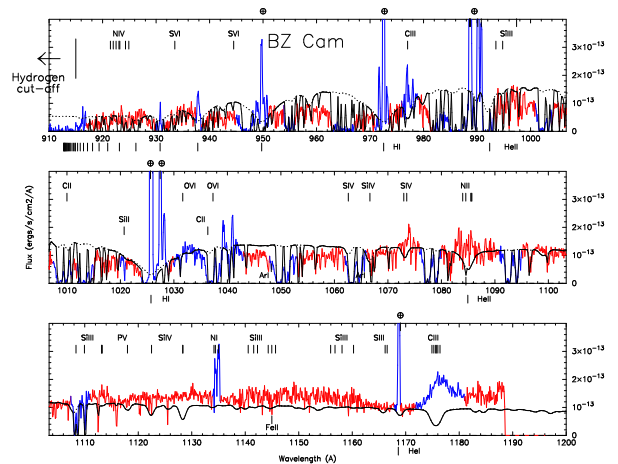


Figure 10. The *FUSE* spectrum of BZ Cam (in red) is fitted with a hot WD to agree with the distance to the system as well as with the flux in the short wavelengths. The WD model (including the ISM absorption model) is drawn as the solid black line, it has $M_{\text{wd}} = 0.4M_{\odot}$, $T_{\text{wd}} = 45,000\text{K}$, solar composition and $V_{\text{rot}} \sin(i) = 200\text{km/s}$ (the same WD model without the ISM absorption model is shown with the dotted black line). The distance obtained from the fit is 791pc. The ISM absorption features as well as airglow emission lines are marked in blue. We have marked some of the prominent absorption lines that are usually observed in accreting WD with a high temperature, these lines are not observed here, a sign that the observed spectrum might have some emission lines on top of the absorption lines or that the photosphere has a low metallicity.

Modeling the IUE Spectrum— The *IUE* spectrum of BZ Cam was modeled with a 12,500K Kurucz model with $\log g = 2.5$ by Prinja et al. (2000), indicating that a standard disk model does not fit the spectrum. Therefore, we do not attempt a standard disk model but instead we use a modified disk model.

We assume a WD mass of $0.4M_{\odot}$, a low inclination ($i = 10^\circ$ & $i = 20^\circ$) and we vary the mass accretion rate from $10^{-10}M_{\odot}/\text{yr}$ to $10^{-8}M_{\odot}/\text{yr}$. We assume a WD radius $R_{\text{wd}} = 1.15 \times 10^9\text{cm}$, actually corresponding a 10,000K $0.4M_{\odot}$ WD (see section 3.2), and we vary the inner disk radius R_0 from $1R_{\text{wd}}$ to $3R_{\text{wd}}$. We keep the

outer part of the disk at an isothermal temperature of 10, 11, or 12,000K.

We find the best modified disk model fit has a mass accretion rate $\dot{M} = 10^{-8.5} M_{\odot}/\text{yr}$, $i = 20^{\circ}$, a disk inner radius $R_0 = 2R_{\text{wd}}$ ($=23,000\text{km}$), and the outer half of the disk is set to an isothermal temperature $T = 10,000\text{K}$. This outer half of the disk has a surface area 3 times larger than the inner half of the disk, making this modified disk model resemble an isothermal disk model. However, in order for this modified disk model to agree with the known distance ($830 \pm 160\text{pc}$), the outer disk radius had to be set at $\sim 0.5 \pm 0.1a$, corresponding to $R_d \approx 22R_{\text{wd}}$. Though such a disk radius is about twice the accepted radius ($0.3a$) in a CV binary, it is still within the limits of the Roche lobe. Choosing an outer disk radius smaller than this value, decreases the scaled distances. The fit is shown in Fig.11.

Since this modified disk model is close to an isothermal disk, we try next an isothermal disk model, with the same inner and outer radii. The isothermal disk model gives very similar results when its temperature is set to 11,000K. In this model, shown in Fig.12, the deficiency in flux in the shorter wavelength range (the Ly α region) is a little more pronounced than in the modified disk model. In the isothermal disk model, the exact value of the inner disk radius, i.e. whether it is 1 or 2 R_{wd} , has very little effect on the results as it only changes the surface area of the disk by a tiny fraction. Also, the value of the WD mass is not taken into account. However, when integrating the luminosity over the surface of the isothermal disk, the resulting mass accretion rate corresponds to $3.7 \times 10^{-9} M_{\odot}/\text{yr}$ for a $0.4M_{\odot}$ mass WD and $2.7 \times 10^{-9} M_{\odot}/\text{yr}$ for a $0.7M_{\odot}$ mass WD.

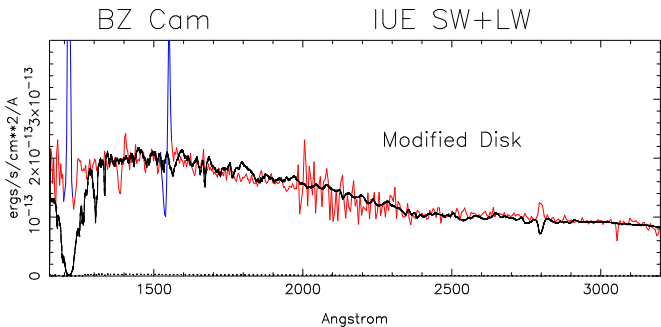


Figure 11. The *IUE* spectrum of BZ Cam (in red, with masked emission lines in blue), is modeled with a modified disk model (in black). The WD mass is $0.4M_{\odot}$, the disk has a mass accretion rate of $\dot{M} = 10^{-8.5} M_{\odot}/\text{yr}$, an inclination $i = 20^{\circ}$, and the outer half of the disk has been set to an isothermal temperature $T = 10,000\text{K}$. The inner disk radius is $R_0 = 2R_{\text{wd}}$ (zero temperature WD), and the outer disk radius is set to 0.5 the binary separation (within the limits of the Roche lobe) in order to match the distance to the system. Note that within the Ly α region the model seems to be deficient in flux.

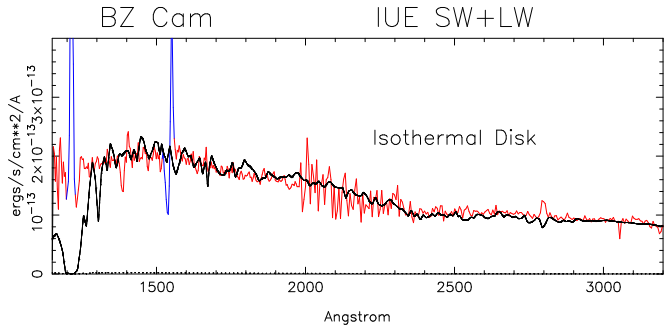


Figure 12. Same as in the previous figure, but now the spectrum is modeled with an isothermal disk only. The disk has a temperature of 11,000K. Here too, in order to scale the model to the known distance, the radius of the disk has to be $0.5a$, departing the most from a standard disk model. The deficiency in flux in the Ly α region is even more pronounced than in the modified disk model.

Self-Consistent Modeling of the *FUSE* & *IUE* Spectra

Since the *FUSE* and *IUE* spectra were obtained years apart, in slightly different brightness states, and with different telescopes/instruments, we do not expect them to match and we do not attempt to combine them. However, when modeling each spectrum separately (*IUE* or *FUSE*), we must take into consideration the results obtained from the modeling of the other spectrum (*FUSE* or *IUE* respectively). Namely, we now model the *IUE* spectrum with a cold disk *and* a hot WD model, similar but not identical, to the WD model obtained from the modeling of the *FUSE* spectrum; and we model the *FUSE* spectrum with a hot WD *and* a cold disk model, similar but not identical, to the cold disk model obtained from the modeling of the *IUE* spectrum.

For the disk model, we choose the isothermal disk model as it is easier to parametrize, and gives results similar to the modified disk model. Namely, the WD mass does not enter the disk model and the WD radius, taken as the inner radius of the disk, has minimum effect on the results. For the WD model, we choose a $0.4M_{\odot}$ WD with a radius increasing with temperature. As we have mentioned earlier, only the WD radius and temperature affects the results.

For the *FUSE* spectrum we find that the 45,000K WD model, with a radius of 18,540km, is improved significantly with the addition of a cold isothermal disk with $T=11,000\text{K}$. The cold disk contributes mainly in the longer wavelengths of the *FUSE* spectrum and helps improve the fit in that region (see Fig.13). The disk has an outer radius of 0.5 the binary separation and the distance obtained from the fit is 854pc. The mass accretion rate obtained by integrating the luminosity of the disk, is $3.7 \times 10^{-9} M_{\odot}/\text{yr}$, and the heated WD luminosity is of the same order.

The fit is improved further by increasing the WD

temperature to 50,000K and the isothermal disk temperature to 12,000K, however the distance increases to 1137pc. This model is shown in Fig.14. The disk integrated luminosity gives a mass accretion $\dot{M} = 5 \times 10^{-9} M_{\odot}/\text{yr}$ and here too the WD luminosity is of the same order.

For the *IUE* spectrum we find that for the model to fit the spectrum, the temperature of the disk has to be decreased as the temperature of the WD increases. The best fit (Fig.15) is obtained for a disk with a temperature of 10,000K combined with a 40,000K WD. This model also gives a distance of the order of 650pc for an outer disk radius $\sim 0.6a$. The integrated luminosity of the disk gives a mass accretion rate of $2.5 \times 10^{-9} M_{\odot}/\text{yr}$, while the WD luminosity is about 10 percent less than that of the disk.

The results of the analysis of the UV spectra of BZ Cam can be summarized as follows: a $0.4M_{\odot}$ WD with a temperature of $45,000 \pm 5,000\text{K}$, and a disk with a temperature of $11,000 \pm 1000\text{K}$, extending to 0.5 ± 0.1 the binary separation. Taking only the disk luminosity into consideration gives a mass accretion rate of the order of $2.5 \times 10^{-9} M_{\odot}$ to $5 \times 10^{-9} M_{\odot}/\text{yr}$, and twice as large when also taking the WD luminosity contribution (assuming that the WD is heated due to the advection of energy from the inner disk). The WD contributes mainly to the *FUSE* spectral range while the cold disk contributes mainly to the *IUE* spectral range. The WD mass could be larger, i.e. $0.7M_{\odot}$, but its radius would have to be of the order of 20,000km, i.e. twice as large as expected for such a mass (again, see section 3.2 for details).

5.3. V592 Cas

We assumed a $0.8M_{\odot}$ WD mass with a radius $R_{\text{wd}} = 7,000\text{km}$, which is consistent with a temperature of such a WD at about 16,000K. The inner radius of the disk, R_0 , was placed at $1.0R_{\text{wd}}$, $1.2R_{\text{wd}}$, $1.5R_{\text{wd}}$, and $2.0R_{\text{wd}}$. The outer radius was placed at $36R_{\text{wd}} \approx a/3$, where a is the binary separation of V592 Cas derived from Table 1. The outer region of the disk was allowed to take different temperatures: either the actual disk temperature, or 10,000 K, 11,000 K, or 12,000 K. The size of that outer region was also varied. Some preliminary modelings were carried out using a grid of standard disk models, to obtain an order of estimate of the mass accretion rate, which gave $\dot{M} \sim 10^{-8} M_{\odot}/\text{yr}$. Modified disk models were then computed within the vicinity of this mass accretion rate assuming an inclination angle of 30° .

The models were chosen to provide the best fit and the correct distance (≈ 350 pc) to the source. The best fit is for a modified disk with a mass accretion rate of $\dot{M} = 10^{-8.2} M_{\odot}/\text{yr}$ ($\sim 6.3 \times 10^{-9} M_{\odot}/\text{yr}$), an inner disk radius placed at $R_0 = 1.2R_{\text{wd}}$, an outer disk radius at $30R_0$, and an isothermal outer disk between $r = 20R_0$ and $r = 30R_0$ with a temperature $T=12,000\text{K}$. A 45,000K WD contribution was added to the model for completeness (Hoard et al. 2009) but contributed only a few percent

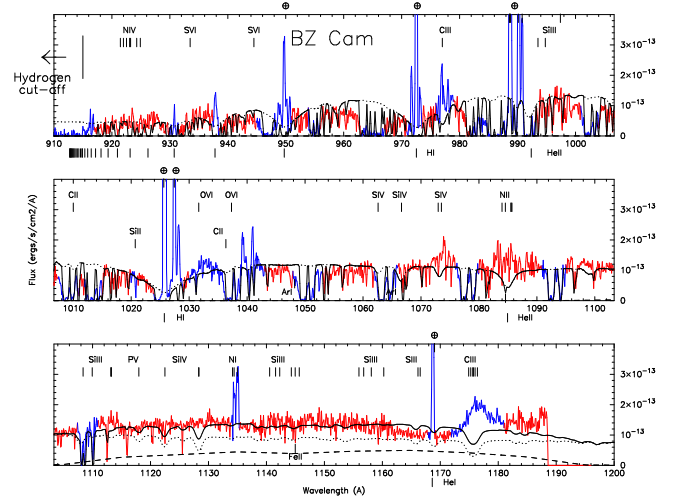


Figure 13. The *FUSE* spectrum of BZ Cam is modeled with $0.4M_{\odot}$ 45,000K WD (dotted line) plus a 11,000K isothermal disk (dashed line) of radius 0.5a. The combined model (solid black line) includes a basic ISM absorption model. Note that the isothermal disk, contributing only 7% of the flux in the *FUSE* range, improves the overall fit and more particularly in the longer wavelength. The distance obtained from the fit is 854pc. The region of the C III (1160-1180) shows a possible P-Cygni profile, though it is also a region exhibiting a detector artifact known as the ‘worm’.

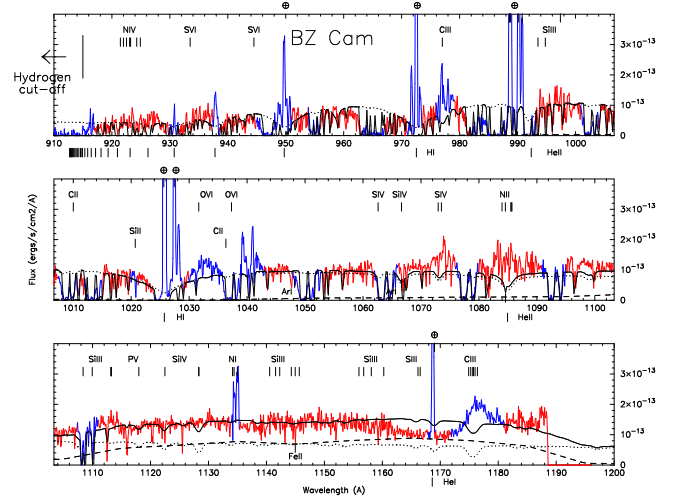


Figure 14. The *FUSE* spectrum of BZ Cam is modeled with $0.4M_{\odot}$ 50,000K WD (dotted line) plus a 12,000K isothermal disk (dashed line). The combined model (solid black line) includes a basic ISM absorption model. The isothermal disk now contributes 25% in the *FUSE* range of the flux, and further improves the fit in the longer wavelength. The distance obtained from the fit is 1137pc.

to the flux and did not affect the model. Consequently, the temperature of the WD could not be assessed from our modeling. The fit is presented in Fig.16 in the *FUSE* spectral range and in Fig.17 in the *IUE* SWP+LWP spectral range.

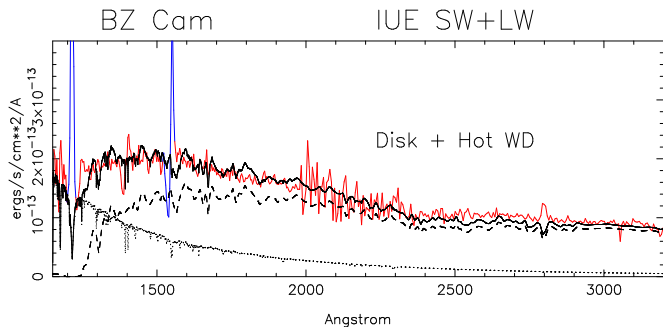


Figure 15. The *IUE* spectrum of BZ Cam is modeled (solid black line) with an isothermal disk plus a hot WD. The disk (dashed black line) has a temperature of 10,000K and the WD (dotted black line) has a temperature of 40,000K. Note that the WD contribution greatly improves the fit in the Ly α region.

For a 16,000K WD with a radius of 7,000km, the modified disk model, with a 8,400km inner radius, starts only at $1.2R_{\text{wd}}$, and for a 45,000K WD with a radius of 7,450km the disk starts at $1.13R_{\text{wd}}$. In either case the size of the BL would be relatively narrow ($\sim 0.1 - 0.2R_{\text{wd}}$) and this modified disk model is very similar to a standard disk model in its inner region, and differs mainly in the assumption of an outer isothermal region. V592 Cas is not a case as extreme as BZ Cam or MV Lyr.

6. DISCUSSION

In the present UV spectral analysis, we find that the data for the UX UMa system V592 Cas are consistent with a slightly modified disk model (very similar to a standard disk) with an inner disk radius at $R_0 = 1.2R_{\text{wd}}$, $\dot{M} = 10^{-8.2}M_{\odot}/\text{yr}$, and an outer 12,000K isothermal disk. The small surface of the $\sim 0.8M_{\odot}$ WD is overshadowed by the disk, as its contribution, even at a temperature $T_{\text{wd}} = 45,000\text{K}$, is negligible. The data for our two VY Scl systems MV Lyr & BZ Cam point to a different scenario. For MV Lyr we find a significantly modified disk model with an inner radius as large as $2R_{\text{wd}}$, and an outer 10,000K isothermal disk. The contribution of the 45,000K $0.8M_{\odot}$ WD is significant. BZ

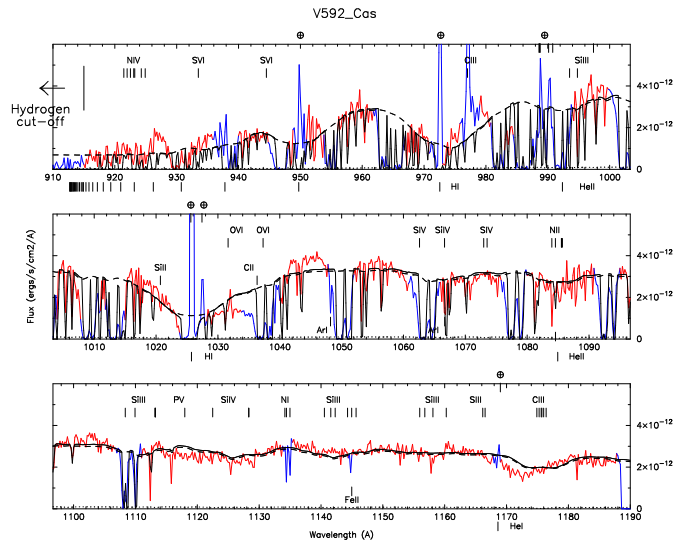


Figure 16. The *FUSE* spectrum of V592 Cas (in red) has been fitted with a combined WD + modified disk model (solid black line). The WD model, dotted line, has a mass of $0.8M_{\odot}$ with a temperature of 45,000K, but contributes very little to the combined model and was added only for completeness. The modified disk model, dashed line, has a mass accretion rate of $6.3 \times 10^{-9}M_{\odot}/\text{yr}$ ($\log(\dot{M}) = -8.2$), with an inclination of 30° . The inner radius of the disk is set at $R_0 = 1.2R_{\text{wd}}$ (8,400 km), and the outer radius is set at $30R_0$. The outer region of the disk between $20R_0$ and $30R_0$ was set to a temperature of 12,000 K. This model gives a distance of 342 pc. The regions affected by ISM absorption features and sharp emission lines (due to day light) are omitted (masked) for the fitting and have been colored in blue. The location of absorption lines observed in the *FUSE* spectra of some CVs have been marked, but are not especially observed here.

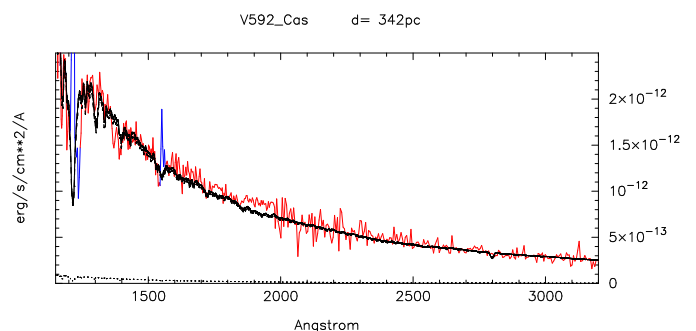


Figure 17. The same disk model shown in Fig.16 is now fitted to the *IUE* spectrum of V592 Cas. For clarity the vertical scale is different than in Fig.16.

Cam is an even more extreme case in that it has a slope shallower than MV Lyr and V592 Cas, and its spec-

trum is consistent with a large cold isothermal disk with $T \sim 10 - 11,000\text{K}$ extending to the limit of the Roche lobe ($\sim 0.5a$). A modified disk model with an inner radius of $2R_{\text{wd}}$ (40,000km) and an extended outer isothermal region provides the same solution. Its $0.4M_{\odot}$ WD with a 20,000km radius, and a temperature of 45,000K contributes most of the flux in the *FUSE* range. For both MV Lyr and BZ Cam the mass accretion rate is about twice as small as for V592 Cas.

The hot WD scenario in the two VY Scl NL systems MV Lyr and BZ Cam, with an inner disk hole $\sim 2R_{\text{wd}}$, is consistent with our recent *Swift* X-ray data analysis which reveals that the optically thin hard X-ray emitting boundary layer is under-luminous, a sign that it cannot radiate its energy to cool efficiently, and, instead, the boundary layer energy is advected into the outer layer of the white dwarf, heating it, possibly inflating its radius and launching an outflow. This is the self-consistent global picture we draw from our present UV spectral analysis and our previous *Swift* X-ray analysis. In this picture, the optically thin BL extends to $r \sim 2R_{\text{wd}}$ and heats the WD through advection of energy. For V592 Cas, the inner hole is much smaller extending only to $\sim 1.2R_{\text{wd}}$.

To further check this scenario, we select a larger and self-consistent set of X-ray data for CVs to compare to the archival *IUE* data. If the above scenario is correct, we expect the systems with UV spectra departing from the standard disk model to have a harder X-ray emission than those systems with UV spectra agreeing with the standard disk model. For this purpose, we turn to [van Teeseling et al. \(1996\)](#), who computed the X-ray hardness ratio from ROSAT observations of non-magnetic cataclysmic variables, including 5 VY Scl NLs and 6 UX UMa NLs observed in a state of high accretion rate, and a number of DN systems observed in their quiescent state. ROSAT has an energy range (0.1-2.4keV) that is *relatively* soft considering that some intermediate polars can be as hard as 20-300keV. In spite of the fact that the DNe were observed in quiescence, [van Teeseling et al. \(1996\)](#) found that the NL VY systems had a X-ray hardness ratio larger than the NL UX UMa and quiescent DN SU UMa systems. DN systems in outburst are known to exhibit hard X-rays too (only a few systems exhibit EUV/soft X-rays). During outburst, however, the X-ray temperature is lower than in quiescence ([Balman 2015](#)). Consequently, the hardness ratio of the quiescent DNe computed in [van Teeseling et al. \(1996\)](#) is an upper limit to hardness ratio of these same DNe in outburst. So the data in [van Teeseling et al. \(1996\)](#) give us the hardness ratio of disk-dominated UX and VY NLs and an upper limit to the hardness ratio of DN in outburst.

As noted by [la Dous \(1991\)](#), disk-dominated NL systems have a shallower UV continuum slope than the DN in outburst and cannot be modeled with standard disk models. To *quantitatively* assess the departure from the standard disk model in the UV, we measure

the slope of the continuum of the *IUE* spectra, flux in $\langle \text{erg/s/cm}^2/\text{\AA} \rangle$ as a function of wavelength in $\langle \text{\AA} \rangle$ on a log-log scale, for the sample of non-magnetic disk systems in [van Teeseling et al. \(1996\)](#) (for which *IUE* data exist). Using the LWP segment and the longer wavelength region of the SWP spectrum past the 1550Å carbon line, we obtain a UV spectral coverage from $\sim 1600\text{\AA}$ to $3,200\text{\AA}$. We deredden all the spectra based on the E(B-V) values from the literature ([Bruch & Engel 1994](#)) or directly from the 2175Å absorption feature using the extinction curve from [Fitzpatrick & Massa \(2007\)](#) with $R = 3.1$. We then measure the slope of the UV continuum directly from the log-log graphs that we generate for these systems (graphs similar in appearance to Figs. 1, 2, & 3). We have here a limited sample of systems as we decided to take only those systems for which the hardness ratio was measured from the same telescope in the same manner and [van Teeseling et al. \(1996\)](#) provides such a self-consistent sample.

In Table 3, we list the ROSAT X-ray hardness ratio and *IUE* UV continuum slope for the 9 DN systems, 6 UX NL systems and 4 VY NL systems together with the novalike V795 Her and the two old novae V603 Aql, and RR Pic. V592 Cas was not included in [van Teeseling et al. \(1996\)](#) and has no hardness ratio listed. MV Lyr is listed twice, once for its intermediate state and once for its high state that exhibits a slightly different UV continuum slopes. At the bottom of the table we also list the UV continuum slope of some standard disk models computed with TLUSTY and SYN-SPEC (e.g. [Wade & Hubeny \(1998\)](#)) for comparison. The standard disk models have a slope that flattens as the mass accretion rate decreases.

Table 3. System Parameters

System Name	Type	UV slope	hardness ratio
WZ Sge	DN/SU	-2.4	0.21
SW UMa	DN/SU	-2.5	0.00
SU UMa	DN/SU	-1.9	0.24
Z Cha	DN/SU	-1.7	0.53
WX Hyi	DN/SU	-2.0	0.46
T Leo	DN/SU	-2.3	0.22
VW Hyi	DN/SU	-2.4	0.05
AB Dra	DN/UG	-2.1	0.84
WW Cet	DN/ZC	-1.75	0.50
RW Tri	NL/UX	-1.8	1.39
AC Cnc	NL/UX	-1.7	-0.26
UX UMa	NL/UX	-2.0	0.05
IX Vel	NL/UX	-2.2	0.10
V3885 Sgr	NL/UX	-2.1	0.38
V592 Cas	NL/UX	-2.4	—
BZ Cam	NL/VY	-1.15	0.95

Table 3 continued

Table 3 (continued)

System Name	Type	UV slope	hardness ratio
KR Aur	NL/VY	-1.55	0.96
MV Lyr i	NL/VY	-1.4	0.83
MV Lyr h	NL/VY	-1.6	0.83
TT Ari	NL/VY	-1.9	0.83
V795 Her	NL/SH	-1.9	0.00
V603 Aql	CN/SH	-2.35	0.83
RR Pic	CN/SW	-1.95	-0.49

System	\dot{M} $< M_{\odot}/yr >$	UV slope	hardness ratio
Standard Disk	$10^{-9.5}$	-2.52	—
Standard Disk	$10^{-9.0}$	-2.89	—
Standard Disk	$10^{-8.5}$	-2.88	—
Standard Disk	$10^{-8.0}$	-2.94	—

NOTE—The subtypes are as in Ritter & Kolb (2003), except for the novae that are denoted CN (classical nova). The UV continuum slope was measured directly from the dereddened *IUE* spectra and the ROSAT X-ray hardness ratio was taken from van Teeseling et al. (1996). Some standard disk models (Wade & Hubeny 1998) are also included for comparison.

In Fig.18 we plot the UV continuum slope of these systems against the ROSAT X-ray hardness ratio reported in van Teeseling et al. (1996). Eventhough the X-ray hardness ratio for DNe is an upper limit, and all the DNe (green triangle) are expected to be located more to the left, had the hardness ratio been measured in outburst, there is a clear separation between DNe and VY Scl systems. Furthermore, for this limited sample, it appears that the VY Scl systems have a shallower UV slope with harder X-ray spectrum, consistent with the scenario of an optically thin inner disk with a modified disk model. The DNe have a softer spectrum and a steeper UV slope consistent with either a standard disk model or a less modified disk model with a less extended optically thin inner disk (e.g. as we found for V592 Cas). There is an overall tendency pointing to the fact that the more disk-dominated CVs depart from the standard disk model in the UV (shallower slope), the harder is their X-ray emission, respectively starting with the DN systems and ending with the VY Scl systems.

Motivated by this findings, and to further check the nature of VY Scl systems, we decided to measure the UV continuum slope for all the available *IUE* archive of disk-dominated CVs. We found 105 CVs with *IUE* spectra taken when the disk-dominated the system and

for which a continuum slope could be measured. Reddening values $E(B-V)$ were taken from Bruch & Engel (1994) when available, or were directly assessed using the 2175Å feature. The UV continuum slope for all

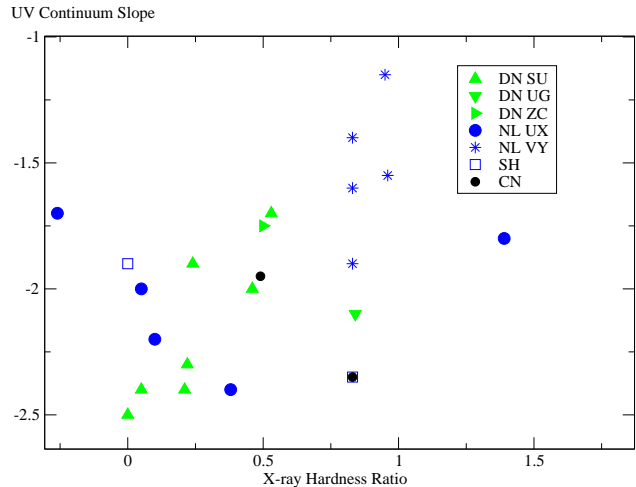


Figure 18. The UV continuum slope of DNe in outburst and NLs in high state (disk-dominated CVs) is plotted against the measured X-ray hardness ratio of quiescent DNe and NLs in high state for the systems listed in Table 3. The subtypes are as indicated in the upper right panel. V603 Aql is here taken both as a CN and as a NL SH. V592 Cas was not included as it is not listed in van Teeseling et al. (1996). DNe in outburst have softer X-ray than in quiescence (Balman 2015), implying that the DNe (green triangles) would shift to the left if the hardness ratio had been measured during outburst. Even so, there is a clear separation between DNe and VY NLs. On the overall, for disk-dominated CVs, the harder is the X-ray, the shallower is the slope of the UV continuum. The departure from the standard disk model in the UV correlates with the X-ray hardness of the system.

the systems was measured after the spectra were dereddened. For each system in Table 4, we list the resulting UV slope together with the Data ID, reddening and orbital period. Some systems with only SWP spectra available were included (V794 Aql and CZ Ori), others were not included because the value of the slope could not be assessed (e.g. V380 Oph). Some systems did not reveal any obvious continuum from which a slope value could be derived, as these spectra were affected by noise, emission lines, or possible additional components (e.g. BH Lyn, V348 Pup, DW UMa). For GI Mon, the only two *IUE* spectra (SWP & LWP) gave a different slope: SWP gave -1.5 and LWP gave -1.1, and the value listed is their average.

We plot the UV continuum slope against the orbital period for all the CVs in Table 4 in two Figures: we show in Fig.19 the systems above the period gap, and in Fig.20 we show the systems below the period gap (for clarity the X-axis has been stretched in Fig.20).

Table 4. UV Continuum Slope of Disk-Dominated Cataclysmic Variables

System Name	Type Subtype	IUE Short	IUE Long	Period $\langle d \rangle$	UV slope	E(B-V)	i $\langle \text{deg} \rangle$
WZ Sge	DN/SU	SP03507	LR03086	0.056694	-2.4	0.00	77
SW UMa	DN/SU	SP27871	LP07754	0.056815	-2.5	0.00	45
WX Cet	DN/SU	SP36511	LP15730	0.05827	-2.3	0.00	—
CC Scl	NL/IP	SP34427	LP14189	0.0584	-2.0	0.00	81
T Leo	DN/SU	SP33646	LP13312	0.05882	-2.3	0.00	65
CP Pup	CN/SH	SP27806	LP07782	0.061264	-2.0	0.20	—
V1159 Ori	DN/SU	SP56781	LP31957	0.06218	-2.2	0.00	—
V436 Cen	DN/SU	SP54246	LP30319	0.062501	-2.7	0.07	65
BC UMa	DN/SU	SP50665	LP28027	0.06261	-2.2	0.00	—
EK TrA	DN/SU	SP09705	LR08446	0.06288	-2.25	0.03	58
TV Crv	DN/SU	SP41842	LP20597	0.0629	-2.6	0.10	—
OY Car	DN/SU	SP25857	LP05906	0.063121	-2.2	0.05	83
VY Aqr	DN/SU	SP21719	LP02366	0.06309	-2.2	0.00	—
ER UMa	DN/SU	SP40947	LP19846	0.06366	-2.05	0.00	—
EX Hya	NL/IP	SP03858	LR03435	0.0682338	-1.6	0.00	78
IR Gem	DN/SU	SP38524	LP17696	0.0684	-2.15	0.00	—
VZ Pyx	DN/SU	SP44128	LP22531	0.07332	-2.35	0.07	—
AY Lyr	DN/SU	SP09342	LR08100	0.0737	-2.4	0.00	—
VW Hyi	DN/SU	SP48680	LP26405	0.074271	-2.4	0.00	—
Z Cha	DN/SU	SP30677	LP10466	0.074499	-1.7	0.00	82
WX Hyi	DN/SU	SP23952	LP04221	0.074813	-2.0	0.01	40
T Pyx	CN	SP33034	LP12791	0.076223	-2.6	0.35	—
SU UMa	DN/SU	SP34824	LP14532	0.07635	-1.9	0.00	—
YZ Cnc	DN/SU	SP03727	LR03308	0.0868	-1.85	0.00	38
V795 Her	NL/SH	SP22901	LP03269	0.1082648	-1.9	0.00	—
V592 Cas	NL/UX	Table 2	Table 2	0.115063	-2.4	0.22	28
TU Men	DN/SU	SP10665	LR09374	0.1172	-2.6	0.08	—
V442 Oph	NL/VY	SP14731	LR11298	0.12433	-2.2	0.20	—
LQ Peg	NL/VY	SP17367	LR13618	0.124747	-2.2	0.00	—
AH Men	NL/SW	SP43037	LP21666	0.12721	-1.85	0.12	—
DN Gem	CN	SP38213	LP17402	0.127844	-1.7	0.10	—
KQ Mon	NL/UX	SP15384	LR11915	0.128	-1.8	0.04	—
MV Lyr	NL/VY	SP07296	LR06288	0.132335	-1.5	0.00	12
SW Sex	NL/SW	SP21533	LP02262	0.134938	-1.0	0.00	>75
HL Aqr	NL/SW	SP23325	LP03647	0.13557	-2.15	0.05	—
TT Ari	NL/VY	SP42147	LP20922	0.137550	-1.9	0.03	—
V603 Aql	CN/SH	SP05758	LR04994	0.138201	-2.35	0.08	13
WX Ari	NL/SW	SP55953	LP31494	0.139351	-1.0	0.00	72
V1315 Aql	NL/SW	SP27096	LP07085	0.13969	-1.1	0.10	82
V1223 Sgr	NL/IP	SP13365	LR10022	0.140244	-2.15	0.15	24
V2400 Oph	NL/IP	SP47007	LP24971	0.142	-2.4	0.40	—
LN UMa	NL/SW	SP40948	LP19847	0.1444	-1.9	0.15	—
V751 Cyg	NL/VY	SP25774	LP05819	0.144464	-1.1	0.20	—
RR Pic	CN/SW	SP06625	LR05687	0.145025	-1.95	0.00	65
PX And	NL/SW	SP39273	LP18414	0.146353	-1.	0.05	—
V533 Her	CN/IP?	SP44805	LP23205	0.147	-1.4	0.03	—

Table 4 continued

Table 4 (*continued*)

System Name	Type Subtype	IUE Short	IUE Long	Period $\langle d \rangle$	UV slope	E(B-V)	i $\langle \text{deg} \rangle$
V425 Cas	NL/VY	SP15267	LR11783	0.1496	-1.5	0.10	25
AO Psc	NL/IP	SP09706	LR08447	0.1496252	-2.2	0.10	—
AB Dra	DN/UG	SP17619	LR13886	0.1520	-2.1	0.10	—
V794 Aql	NL/VY	SP50754	—	0.1533	-2.1	0.10	—
BP Lyn	NL/SW	SP32940	LP12690	0.152812	-2.1	0.00	—
BZ Cam	NL/VY	Table 2	Table 2	0.15353	-1.15	0.05	—
LX Ser	VY/SW	SP08070	LR07037	0.158432	-1.0	0.00	90
CY Lyr	DN/UG	SP21030	LR16779	0.1591	-2.5	0.15	—
CM Del	NL/UX	SP14707	LR11282	0.162	-1.9	0.09	73
KT Per	DN/UG	SP17712	LR13968	0.16265777	-2.7	0.20	—
KR Aur	NL/VY	SP14734	LR11299	0.16280	-1.55	0.05	38
AR And	DN/UG	SP18877	LR14885	0.16302	-2.4	0.02	—
CN Ori	DN/UG	SP32593	LP12364	0.163199	-2.15	0.00	67
X Leo	DN/UG	SP15951	LR12282	0.1646	-2.4	0.00	—
VW Vul	DN/ZC	SP18875	LR14883	0.16870	-2.1	0.15	—
UZ Ser	DN/ZC	SP15078	LR11605	0.173	-3.0	0.25	—
V405 Aur	NL/IP	SP56765	LP31949	0.17345	-0.5	0.15	<5
LS Peg	NL/IP	SP39782	LP18948	0.174774	-1.7	0.04	30
WW Cet	DN/ZC	SP10664	LR09373	0.1758	-1.75	0.03	54
U Gem	DN/UG	SP10327	LR08987	0.17690619	-2.5	0.04	70
GI Mon	CN/IP	SP38419	LP17709	0.1802	-1.3	0.10	—
SS Aur	DN/UG	SP18610	LR14679	0.1828	-2.4	0.08	38
DQ Her	NL/IP	SP09201	LR07981	0.19362	-0.75	0.08	90
IX Vel	NL/UX	SP18578	LR14657	0.193927	-2.2	0.01	57
UX UMa	NL/UX	SP46816	LP24773	0.196671	-2.0	0.02	70
FO Aqr	CN/IP	SP15260	LR11774	0.202	-0.5	0.00	—
V825 Her	NL/UX?	SP17353	LR13601	0.206	-2.0	0.00	—
HX Peg	DN/ZC	SP37458	LP16654	0.2008	-2.0	0.00	—
V3885 Sgr	DN/UX	SP25655	LP05709	0.207161	-2.1	0.02	—
RX And	DN/ZC	SP17673	LR13942	0.209893	-2.1	0.02	51
PQ Gem	NL/IP	SP46993	LP24965	0.211636	-0.5	0.00	low
HR Del	CN	SP02122	LR02606	0.214165	-2.6	0.17	40
CZ Ori	DN/UG	SP07385	—	0.214667	-2.35	0.00	—
TV Col	NL/IP	SP08672	LR07425	0.2286	-2.2	0.02	70
RW Tri	NL/UX	SP07915	LR06895	0.231883	-1.8	0.10	71
VY Scl	NL/VY	SP32594	LP12365	0.2323	-1.9	0.06	30
TX Col	NL/IP	SP00502	LP11930	0.23825	-1.55	0.05	—
RW Sex	NL/UX	SP26313	LP06299	0.24507	-2.0	0.02	34
AH Her	DN/ZC	SP17671	LR13923	0.258116	-2.2	0.03	46
TZ Per	DN/ZC	SP17643	LR13907	0.262906	-2.45	0.27	—
TW Pic	NL/VY	SP27087	LR17818	0.265	-2.3	0.05	—
TT Crt	DN/UG	SP47801	LP25680	0.2683522	-2.3	0.00	—
SS Cyg	DN/UG	SP48441	LP26199	0.27513	-2.5	0.07	51
Z Cam	DN/ZC	SP26717	LP15337	0.2898406	-2.0	0.02	57
EM Cyg	DN/ZC	SP07297	LR06289	0.290909	-2.1	0.03	67
AC Cnc	NL/UX	SP18735	LR14787	0.300478	-1.7	0.00	76

Table 4 *continued*

Table 4 (*continued*)

System Name	Type Subtype	IUE Short	IUE Long	Period $\langle d \rangle$	UV slope	E(B-V)	i $\langle \text{deg} \rangle$
V363 Aur	NL/UX	SP25335	LP05437	0.321242	-1.9	0.15	70
BT Mon	CN/SW	SP25446	LP05516	0.333814	-2.2	0.24	82
RZ Gru	NL/UX	SP15385	LR11916	0.360	-1.75	0.03	—
RU Peg	DN/UG	SP15079	LR11606	0.3746	-2.1	0.00	43
SY Cnc	DN/ZC	SP08082	LR07051	0.38	-2.3	0.00	—
KO Vel	NL/IP	SP16034	LR12341	0.422	-1.4	0.05	—
DX And	DN/UG	SP37687	LP16843	0.440502	-1.9	0.10	45
QU Car	NL/UX	SP41926	LP20699	0.45	-2.3	0.11	<60
DI Lac	CN	SP29325	LP09208	0.543773	-2.0	0.26	—
V841 Oph	CN	SP07950	LR06925	0.601304	-2.6	0.40	—
BV Cen	DN/UG	SP24867	LP05162	0.610108	-1.5	0.10	53
GK Per	NL/IP	SP20653	LR16563	1.996803	-0.7	0.30	<73

NOTE—We List here 105 cataclysmic variables for which an *IUE* spectrum was taken when the system was dominated by emission from the disk. The CV subtypes are according to Ritter & Kolb (2003), except for the novae which we denote as systems having experienced a classical nova explosion (CN). The reddening values E(B-V) were taken from Bruch & Engel (1994) of directly assessed based on the 2175Å absorption feature. The slope of the UV continuum was assessed for each system after the spectra were dereddened using the relation from Fitzpatrick & Massa (2007) with R=3.1. Periods and inclinations are also taken from the Ritter & Kolb Catalogue (Ritter & Kolb 2003).

On the overall, the DNe present the steepest average slope (-2.20 to -2.27) and, therefore, their disk departs from the standard disk model less than the NLs with an average slope of -1.99 to -1.63. Not surprisingly, the intermediate polars, with their magnetically truncated inner disks, have the shallowest average slope of all, with a value of only -1.43, with a very large scatter ranging from -0.5 to almost -2.5. This is consistent with the suggestion that the slope of the UV continuum becomes shallower as the size of the inner hole in the disk increases. We note, however, that the eclipsing SW Sex stars, with an average slope value of -1.63, seems to cluster around either -2.0 or -1.0.

The small number of DNe that are showing soft X-ray emission in outburst (van Teeseling et al. 1996; Kuulkers et al. 2006), VW Hyi, OY Car, SW UMa, SS Cyg, U Gem, and Z Cam, all exhibit a rather steep UV slope: -2.4, -2.2, -2.5, -2.5, -2.5, and -2.0 respectively. The average value of their UV slope is -2.35, while the average value of the VY Scl with the hardest X-ray emission of all CVs is -1.70, again pointing to the fact that the slope of the UV spectral continuum increases with the softness of the X-ray emission.

We now consider the UV slope by CV subtype, excluding the magnetic IPs and eclipsing SW Sex stars, we obtain the following sequence in order of decreasing steepness of the average UV slope: SU UMa and U Gem systems (~ -2.26), Z Cam systems (-2.20), UX UMa systems (-1.99), and VY Scl systems (-1.70).

This sequence is the same for the ratio of the X-ray flux to optical flux and/or UV flux of CVs in decreasing order: from ~ 0.1 for SU UMa systems, to U Gem systems, to ~ 0.01 for Z Cam systems, to ~ 0.001 for UX UMa systems and VY Scl systems in high state (Balman 2015; Kuulkers et al. 2006), which is due mainly to an increase of the optical/UV flux (or \dot{M}). Within the context of our modified disk model, a simple interpretation of this correlation is that the optically thin advective inner disk/BL region increases with decreasing mass accretion rate.

From Figs. 19 & 20, we also find that for the all the DNe, separately above and below the gap, the slope value is *possibly increasing slightly* (less negative) with increasing orbital period: the UV slope increases from -2.5 at an orbital period of $P \sim 0.15\text{d}$ to -2.0 at $0.3\text{d} < P < 0.6\text{d}$, above the gap (Fig.19); and a similar increase is noticeable below the period gap, from -2.5 at $P \sim 0.06\text{d}$ to -2.0 at $P \sim 0.075\text{d}$ (Fig.20). The increase of the UV slope value as a function of the orbital period, for the DN systems, is a *weak* correlation, and it seems to be counter intuitive as one would expect larger mass accretion rate systems, at longer orbital period, to have a disk that is hotter with a steeper UV slope. However, the size of the disk also increases with increasing binary separation at longer orbital period, thereby increasing the surface area of the colder outer disk, providing a possible explanation for the increase of the UV slope value. This is similar to our modified disk modeling, where the increasing size

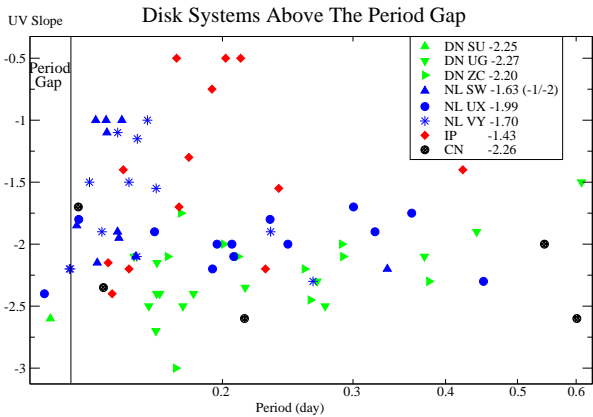


Figure 19. The slope of the (*IUE*) UV continuum is shown as a function of the orbital period (in days, on a log scale) for the disk-dominated CV systems listed in Table 4. For clarity, only the region above the period gap is shown extending to $P \sim 0.6$ days. The subtypes are shown as indicated by the different symbols and colors in the panel on the upper right, where the average value of the slope is also listed for each subtype. On the overall DNe SU, UG & ZC subtypes (all in green) have all a similar average slope of about ~ -2.25 , significantly steeper than the NLs (shown in blue). The UX UMa NLs have an average slope of about -2 , the VY Scl NLs have an average slope of -1.70 , and the eclipsing SW Sex NLs seem to cluster around either -1.0 or -2.0 with an average value of -1.63 . The intermediate polars have been included (in red) for comparison and have an average slope of only 1.43 (with a very broad scattering) not inconsistent with magnetically truncated inner disks. For the DNe UG & ZC (as a whole), the steepest (most negative) slope value reached at a given orbital period shows an increase (less negative) with orbital period. The SU UMa systems below the gap, shown in detail in Fig.20, exhibit a similar pattern. We included the novae (CN) classified as IP (CN/IP) with the IPs, thereby, leaving only 7 CN systems.

and the cold temperature ($\sim 10 - 12,000$ K) of the outer disk also makes the UV continuum slope shallower.

It has been cautioned that systems with a higher inclination may exhibit a flatter UV continuum slope (la Dous 1991), however, we find that this does not seem to be the case. In fact there seems to be a selection effect showing the opposite, as most of the VY Scl systems (characterized by a shallow UV continuum slope) in our sample have a low inclination (< 40 deg) while most of the remaining non-magnetic systems (with a steeper UV continuum slope) in our sample have a higher inclination, making appears as if the low inclination systems have a shallow UV slope. Many systems in Table 4 do not have a known inclination, nevertheless, we draw the UV continuum slope against the inclination in Fig.21. There do not appear to be an obvious correlation between the UV slope and the inclination, except maybe at a very high inclination, where 3 SW Sex NL system cluster around -1 (e.g. LX Ser). The IPs systems exhibiting the shallowest slope of all (-0.5 to -0.7) do not especially have a high inclination: FO Aqr has $i = 65$ deg and GK Per, $i \sim 46 - 73$ deg, but V405 Aur has $i < 5$ deg, and PQ Gem has a low (but unknown) inclination. The

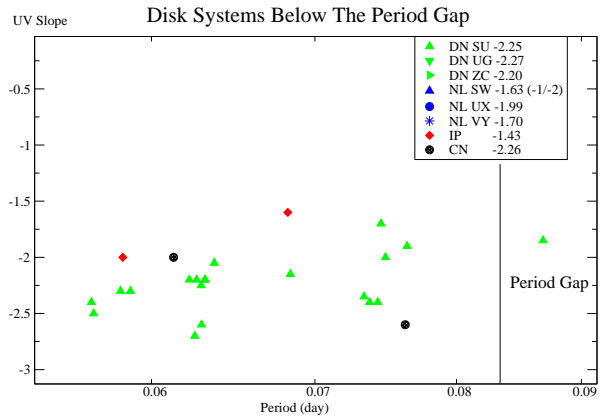


Figure 20. The UV slope against the orbital period is shown, as in Fig.19, but for the SU UMa systems below the period gap. The horizontal (log) axis has been stretched for clarity. As for the the U Gem and Z Cam systems, the steepest slope value reached for the SU Uma's at a given orbital period shows an increase with orbital period, and overall the UV slope value for the SU UMa systems slightly increases (less shallow) with orbital period.

same is true for the VY Scl systems: V425 Cas with a slope of -1.5 has an inclination of only 25 deg, BZ Cam with a slope of -1.15 has an inclination less than 40 deg.

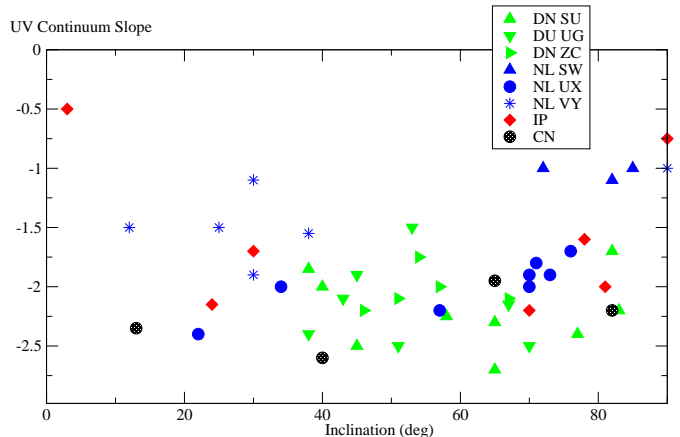


Figure 21. The UV slope against the inclination of the system is shown for the CVs in Table 4 for which the inclination is known. Except, possibly, for the few systems close to 90 deg, there does not appear to be a correlation between the UV slope and the inclination.

7. SUMMARY AND CONCLUSION

Our spectral analysis demonstrate that the two VY Scl systems MV Lyr and BZ Cam, departing from the standard disk model in the UV range (with a shallow UV continuum slope of -1.4 and -1.15 respectively), can be modeled with a modified/truncated inner disk (of size

$\sim R_{\text{wd}}$) and a hot WD with an inflated radius. The UX UMa NL system V592 Cas, with a steeper UV continuum slope of -2.4, is modeled with a less modified disk model with a smaller truncated inner disk region (at $\sim 1.2R_{\text{wd}}$). The picture we present, to justify our modified (truncated) inner disk, is that of a geometrically extended, of size up to $\sim R_{\text{wd}}$, optically thin BL/inner disk heating the WD through advection of energy, and which provides an explanation for the observed UV and X-ray data in a self-consistent manner. This scenario is further strengthened by the correlation we found: the non-magnetic disk systems (i.e. excluding quiescent DNe) exhibiting the hardest X-ray (the VY Scl systems in our sample in Table 3) have also the shallowest UV slope, while at the other end, the disk systems exhibiting soft X-ray (5 DNe in outburst) have a much steeper UV slope.

We find that the UV continuum slope of the SW Sex systems is possibly affected by their high inclination. As to the magnetically truncated inner disk systems, the IPs, they have the shallowest UV slope of all CVs, consistent with the proposed modified disk models with a truncated inner region providing a shallower UV continuum slope.

In addition, many NL systems exhibit hot, fast wind outflows seen in P Cygni line structure and blue-shifted absorption. These winds originate in the inner disk/BL region, with some systems revealing ejected nebular material (e.g. BZ Cam, Ellis et al. (1984)). Also, our X-ray analysis of the NLs MV Lyr, BZ Cam, & V592 Cas (Balman et al. 2014), suggests that these systems have optically thin BLs possibly merged with ADAF-like flows and/or hot coronae.

The X-ray (hard spectra) and UV characteristics (shallow slope) of NL VY systems, including their unexpected hot WD (Pala et al. 2017), can be explained with the presence of a geometrically extended optically thin boundary layer/inner disk. When an accretion flow cannot cool efficiently, due to being optically thin, the energy is advected with the flow into the outer layer of the star (Abramowicz et al. 1995), increasing the WD temperature, and likely driving an outflow as in ADAFs (Narayan & Yi 1995). For this reason, we expect the VY Scl systems to be modeled with the modified disk model and the addition of a hot WD, possibly with an inflated radius. The modeling of such systems has to be carried out by creating modified disk models suited to each system individually, taking into account the WD mass, inner and outer disk radius and the binary separation, itself depending on the secondary mass and orbital period. We note that Balman & Revnivtsev (2012) have shown the existence of a truncated inner disk in quiescent dwarf novae as well, where the flow changes from optically thick into a hot ADAF-like flow. Since quiescent dwarf novae have a very low \dot{M} , the optical thickness in the BL must be very small and the truncation radius relatively large.

The UX UMa systems have an average slope some-

what intermediate between that of VY Scl systems and DNe in outburst. Namely, their disk (e.g. V592 Cas) is less modified than for the VY Scl subtype. As to the DN systems, as a whole, below and above the period gap, they have an average UV continuum slope closest to the standard disk and should be modeled with only minimal disk modifications. Their disk has a geometrically small and optically thin inner disk/BL region.

We have proposed here a modified disk model compatible with the X-ray and UV characteristics of non-magnetic CVs, that provides a possible explanation for the discrepancy between the data and theory, simultaneously in the UV (shallow UV slope) and in the X-ray (optically thin and missing BL). We found, by carrying out a quantitative assessment, that the UV and X-ray data self-consistently support this scenario, and suggest that the size of the optically thin inner hole (and advection process) in the disk *might be* increasing in the following sequence: SU UMa and U Gem systems, followed by Z Cam systems, UX UM systems, and VY Scl systems. In addition, this scenario explains several of the characteristics unique to the VY Scl systems, such as their elevated WD temperature and ejected nebular material.

To complete this conclusion, we observe that the optical spectra of disk-dominated CVs also show a continuum slope that is rather shallow when compared to theoretical disk spectra, and the Balmer edge (around $\sim 3700\text{-}4000\text{\AA}$) is often not detected, or it is seen in absorption but its size is smaller than expected (la Dous 1989). It has been suggested that some of the accretion energy possibly goes in the formation of a disk wind contributing to the UV and optical continuum. Matthews et al. (2015) have shown that the inclusion of such a disk wind significantly improves the spectral fit of the model to the observed UV and optical spectra and fills up the Balmer edge, thereby explaining its non-detection in many optical spectra of disk-dominated CVs and providing a viable explanation for the observed features of UV and optical spectra in CVs. Our present research does not take into account emission from a disk wind as it is limited to the emission from the optically thick disk. In this context our disk model with a truncated inner region comes as the disk contribution to which a disk wind contribution has to be added to provide a more complete picture. In our modeling (see section 3.7) we include an isothermal outer disk region with an elevated temperature as the impinging of the L1-stream on the rim of the disk and the tidal interaction from the secondary are expected to heat the outer region of the disk (Buat-Ménard et al. 2001). Irradiation from the hot inner boundary layer could also contribute to heating of the outer disk. It is possible that the isothermal outer disk partially compensates for the lack of disk wind emission in our modeling.

We wish to thank The Astrophysical Journal Editor Allen Shafter for his promptness in handling the manuscript, and in particularly the referee, Ivan

Hubeny, for his short constructive and encouraging comments and promptness in delivering a report that helped expedite the article. This work was supported by the National Aeronautics and Space Administration (NASA) under grant numbers NNX17AF36G, NNX13AF11G & NNX13AF12G issued through the Office of Astrophysics Data Analysis Program (ADAP)

and grant number NNX13AJ70G issued through the Astrophysics Division Office (*Swift* Cycle 8 Guest Investigator Program) all to Villanova University. We have used some of the online data from the AAVSO, and are thankful to the AAVSO and its members worldwide for making this data public and their constant monitoring of cataclysmic variables.

REFERENCES

- Araujo-Betancor, S., et al. 2005, *ApJ*, 622, 589
- Abramowicz, M.A., Chen, X., Kato, S., Lasota, J.-P., & Regev, O. 1995, *ApJ*, 438, L37
- Balbus, S.A., & Hawley, J.F. 1991, *ApJ*, 376, 214
- Balman, S. 2015, *Acta Polytechnica CTU proceedings*, Vol.2, p.116
- Balman, S., Godon, P., Sion, E.M. 2014, *ApJ*, 794, 84
- Balman, S., & Revnivtsev, M. 2012, *A&A*, 546, A112
- Baskill, D.S., Wheatley, P.J., Osborne, J.P. 2005, *MNRAS*, 357, 626
- Bruch, A., & Engel, A. 1994, *A&AS*, 104, 79
- Buat-Ménard, V., Hameury, J.-M., & Lasota, J.-P. 2001, *A&A*, 366, 612
- Cardelli, J.A., Clayton, G.C., Mathis, J.S. 1989, *ApJ*, 345, 245
- Chiappetti, L., Maraschi, L., Treves, A., & Tanzi, E.G. 1982, *ApJ*, 258, 236
- Córdova, F.A., Mason, K.O., & Nelson, J.E. 1981, *ApJ*, 245, 609
- la Dous, C. 1989, *MNRAS*, 238, 935
- la Dous, C. 1990, in *Cataclysmic Variables and Related Objects*, M. Hack (ed.), NASA/CNRS Monograph Series on Non-Thermal Phenomena in Stellar Atmospheres, p.14
- la Dous, C. 1991, *A&A*, 252, 100
- Dixon, W.V., et al. 2007, *PASP*, 119, 527
- Ellis, G.L., Grayson, E.T., Bond, H.E., 1984, *PASP*, 96, 283
- Ferland, G.J., Pepper, G.H., Langer, S.H., MacDonoald, J., Truran, J.W., & Shaviv, G. 1982, *ApJ*, 262, 53
- Fitzpatrick, E.L. 1999, *PASP*, 111, 63
- Fitzpatrick, E.L., & Massa, D. 2007, *ApJ*, 663, 320
- Froning, C., Long, K.S., Gänsicke, B.T., Szkody, P. 2012, *ApJS*, 199, 7
- Gänsicke, B.T., Szkody, P., Howell, S.B., Sion, E.M., 2005, *ApJ*, 629, 451
- Garnavitch, P., Szkody, P. 1988, *PASP*, 100, 1522
- Godon, P. 1996, *ApJ*, 463, 674
- Godon, P., Sion, E.M., Barrett, P.E., & Szkody, P. 2009, *ApJ*, 701, 1091
- Godon, P., Sion, E.M., Levay, K., Linnell, A.P., Szkody, P., Barrett, P.E., Hubeny, I., Blair, W.P. 2012, *ApJS*, 203, 29
- Godon, P., Sion, E.M., Linnell, A., Szkody, P., & Hubeny, I. 2008, *ApJ*, 679, 1447
- Godon, P., Sion, E.M., Barrett, P., & Szkody, P. 2007, *ApJ*, 656, 1092
- Greiner, J. et al. 2001, *A&A*, 376, 1031
- Griffith, D., Fabian, D., Sion, E.M. 1995, *PASP*, 107, 856
- Hack, M., & la Dous, C. 1993, *Cataclysmic Variables and Related Objects*, NASA SP-507, US Gov. Printing Office, Washington DC
- Hameury, J.-M., & Lasota, J.-P. 2002, *A&A*, 394, 231
- Hameury, J.-M., Lasota, J.-P., & Warner, B. 2000, *A&A*, 353, 244
- Hamilton, R., et al. 2007, *ApJ*, 667, 1139
- Hoard, D.W., Linnell, A.P., Szkody, P., Fried, R.E., Sion, E.M., Hubeny, I., & Wolfe, M.A. 2004, *ApJ*, 604, 346
- Hoard, D.W., et al. 2009, *ApJ*, 693, 236
- Hollis, J.M., Oliverson, R.J., Wagner, R.M., & Feibelman, W.A. 1992, *ApJ*, 393, 217
- Honeycutt, R.K., Kafka, S., & Robertson, J.W. 2013, *AJ*, 145, 45
- Hubeny, I. 1988, *Comput.Phys.Commun.*, 52, 103
- Hubeny, I. 1990, *ApJ*, 351, 632
- Hubeny, I., & Lanz, T. 1995, *ApJ*, 439, 875
- Hubeny, I., & Lanz, T. 2017a, *A brief introductory guide to TLUSTY and SYNSPEC*
arXiv:1706.01859
- Hubeny, I., & Lanz, T. 2017b, *TLUSTY User's Guide II: Reference Manual*
arXiv:1706.01935
- Hubeny, I., & Lanz, T. 2017c, *TLUSTY User's Guide III: Operational Manual*
arXiv:1706.01937
- Hubeny, I., Lanz, T., & Jeffrey, S. 1994, *St. Andrews Univ. Newsletter on Analysis of Astronomical Spectra*, 20, 30
- Huber, M.E., Howell, S.B., Ciardi, D.R., & Fried, R. 1998, *PASP*, 110, 784
- Kafka, S., Howard, D.W., Honeycutt, R.K., & Deliyannis, C.P. 2009, *AJ*, 137, 197
- Kato T., 2002, *A&A*, 384, 206
- Kluźniak, 1987, PhD Thesis, Stanford University
- Knigge, C. & Long, K. 2002, *ApJ*, 579, 725
- Krautter, J., Klaas, U., & Radons, G. 1987, *A&A*, 181, 373
- Kuulkers, E., Norton, A., Schwope, A., & Warner, B. 2006, in *Compact Stellar X-ray Sources*, ed. W. Lewin & M. van der Klis (Cambridge Astrophysics Series No.39; Cambridge: Cambridge Univ. Press), 421
- Linnell, A.P., Szkody, P., Gänsicke, B.T., Long, K.S., Sion, E.M., Hoard, D.W., & Hubeny, I. 2005, *ApJ*, 624, 923
- Linnell, A.P., Godon, P., Hubeny, I., Sion, E.M., Szkody, P. 2007, *ApJ*, 662, 1204
- Linnell, A.P., Godon, P., Hubeny, I., Sion, E.M., & Szkody, P., Barrett, P.E. 2008, *ApJ*, 676, 1226
- Linnell, A.P., Godon, P., Hubeny, I., Sion, E.M., & Szkody, P. 2010, *ApJ*, 719, 271
- Long, K.S., Wade, R.A., Blair, W.P., Davidsen, A.F., & Hubeny, I. 1994, *ApJ*, 426, 704
- Long, K.S., Sion, E.M., Gänsicke, B.T., Szkody, P. 2004, *ApJ*, 602, 948
- Lu, W., Hutchings, J.B. 1985, *PASP*, 97, 990
- Lynden-Bell, D., & Pringle, J.E. 1974, *MNRAS*, 168, 303
- Matthews, J.H., Knigge, C., Long, K.S., Sim, S.A., Higginbottom, N. 2017, *MNRAS*, 450, 3331
- Mauche, C.W., Raymond, J.C., & Mattei, J.A., 1995, *ApJ*, 446, 842
- Mukai, K., Zietsman, E., & Still, M. 2009, *ApJ*, 707, 652
- Narayan, R., & Popham, R. 1993, *Nature*, 362, 820
- Narayan, R., & Yi, I. 1995, *ApJ*, 444, 231
- Pajdosz, G., Zoha, S. 1992, in Kondo Y., Sistero R., Polidan R.S. eds., *Proc. IAU SYmp. 151, Evolutionary Processes in Interacting Binary Stars*, Kluwer, Dordrecht, p.441
- Pala, A.F., Gänsicke, B.T., Townsley, D. & 28 authors, 2017, *MNRAS*, in press

- Pandel, D., Córdoba, F.A.C.D., Mason, K.O., Priedhorsky, W.C. 2005, ApJ, 626, 396
- Patterson, J., Patino, R., Thorstensen, J.R., Harvey, D., Skillman, D.R., Ringwald, F.A. 1996, AJ, 111, 2422
- Patterson, J., & Raymond, J.C. 1985a, ApJ, 292, 535
- Patterson, J., & Raymond, J.C. 1985b, ApJ, 292, 550
- Popham, R. 1999, MNRAS, 308, 979
- Popham, R., & Narayan, R., 1995, ApJ, 442, 337
- Pringle, J.E., 1977, MNRAS, 178, 195
- Pringle, J.E., 1981, ARAA, 19, 137
- Pringle, J.E., & Savonije, G., 1979, MNRAS, 197, 777
- Prinja, R.K., Ringwald, F.A., Wade, R.A., Knigge, C. 2000, MNRAS, 312, 316
- Prinja, R.K., Knigge, C., Whiterick, D.K., Long, K.S., Brammer G. 2004, MNRAS, 355, 137
- Puebla, R.E., Diaz, M.P., **Hubeny**, I. 2007, ApJ, 134, 1923
- Ringwald, F.A., & Naylor, T. 1998, AJ, 115, 286
- Ritter, H., & Kolb, U. 2003, A&A, 404, 301 (update RKcat7.24, 2016)
- Schneider, D.P., Young, P., & Sheckman, S.A. 1981, ApJ, 245, 644
- Shakura, N.I., & Sunyaev, R.A. 1973, A&A, 24, 337
- Skillman, D.R., Patterson, J., & Thorstensen, J.R. 1995, PASP, 107, 545
- Szkody, P., & Downes, R.A. 1982, PASP, 94, 328
- Szkody, P., Nishikida, K., Raymond, J.C. et al. 2002, ApJ, 574, 942
- van Teeseling, A., Beuermann, K., Verbunt, F. 1996, A&A, 315, 467
- Taylor, C.M., Thorstensen, J.R., Patterson, J., et al. 1998, PASP, 110, 1148
- Tylenda, R. 1981, Acta Astron., 31, 267
- Urban, J., & Sion, E.M. 2006, ApJ, 642, 1029
- Verbunt, F. 1987, A&AS, 71, 339
- Wade, R.A. 1984, MNRAS, 208, 381
- Wade, R.A. 1988, ApJ, 335, 394
- Wade, R.A., & Hubeny, I. 1998, ApJ, 509, 350
- Warner, B. 1995, Cataclysmic Variable Stars, CUP
- Witherick, D.K., Prinja, R.K., Howell, S.B., & Wagner, R.M. 2003, MNRAS, 346, 861
- Woods, J.A., Drew, J.E., Verbunt, F. 1990, MNRAS, 245, 323
- Woods, J.A., Verbunt, F., Cameron, A.C., Drew, J.E., & Pitters, A. 1992, MNRAS, 255, 237
- Wood, M.A. 1995, in White Dwarfs, Proc. 9th Europ. Workshop on WDs, eds. D. Koester & K. Werner (Lecture Notes in Physics, Vol.443; Berlin: Springer), 41